Joint Centre for Mesoscale Meteorology, Reading, UK

Mesoscale Modelling Newsletter
Number 5

Internal Report No. 32

May 1994

Met Office Joint Centre for Mesoscale Meteorology Department of Meteorology
University of Reading PO Box 243 Reading RG6 6BB United Kingdom
Tel: +44 (0)118 931 8425 Fax: +44 (0)118 931 8791
www.metoffice.com

MESOSCALE MODELLING NEWSLETTER

Number 5

May 1994

Issued by the

UK Meteorological Office

CONTENTS

EDITORIAL

S P Ballard
Met Office Unit, Joint Centre for Mesoscale Meteorology
University of Reading

This is the fifth newsletter containing reports from users of the UK Met Office mesoscale models. As last year , reports are also included from other scientists working within the UK in the field of mesoscale and convective scale modelling.

The first four papers report on use and development of the UK Met Office Unified Model, the following two papers use the semi-lagrangian version of the UK Met Office nonhydrostatic mesoscale model. The next three papers use the original UK Met Office nonhydrostatic model and the following two use the UK Met Office Large Eddy Model. The final report uses the Clark anelastic mesoscale model.

The Met Office no longer provides support to outside groups for use of the nonhydrostatic model . However a portable version of the Unified Model code will be made available for use by interested outside groups. Anyone interested should contact A Dickinson, FR Division, UK Met Office, London Road, Bracknell, RG12 2SZ.

Improvements to the Meteorological Office Operational Mesoscale Model

Peter A. Clark
and members of the
Mesoscale Modelling and Assimilation Group
Forecasting Research Division
Meteorological Office, London Road, Bracknell, RG12 2SZ
email: paclark@email.meto.govt.uk

The development and testing of the mesoscale version of the Met Office Unified Model (UM), henceforth referred to as the MM, was described by Ballard *et al* in the last JCMM Mesoscale Modelling Newsletter. It finally went operational in December 1992. Since that time work has continued to improve the model in a number of areas. This work has resulted in several changes to the operational model which were implemented at various stages in the autumn of 1993, and a major change to the operational procedure (continuous assimilation) will be implemented in spring 1994.

The MM went operational after having met specified user requirements for precipitation, 10 m wind and screen temperature (though not, naturally, without plenty of scope for improvement). However, no requirements were specified for its performance with respect to visibility, fog and low cloud. These had been handled quite well by the old Mesoscale Model (OMM) which had higher vertical resolution in the boundary layer and an explicit treatment of aerosol analysis and transport. Not surprisingly, therefore, the performance of the MM when forecasting fog and low cloud was inferior to the OMM. On occasion the model failed to indicate any fog formation when widespread fog was present over much of the country, while on some (less frequent) events spurious fog was predicted. This had inevitable consequences for forecaster confidence in the model. A significant fraction of the work on the model has therefore been directed towards improving the fog and low cloud performance and output products. In addition, considerable effort has gone into reducing the resource requirements of the model.

Implemented Changes

∇^4 diffusion for u, v, θ and humidity: Shortly after becoming operational a few instances occurred of numerical instability in the model. As might be expected these occurred in strong wind situations, with particularly strong upper level jets and surface gradients. The pragmatic approach to curing this problem is to increase the damping introduced by artificial diffusion in the model. However, if this is achieved simply by increasing the artificial diffusion coefficient mesoscale detail will be lost unnecessarily. Increasing the order of diffusion is analogous to increasing the order of filtering, so that the high frequency cutoff is sharper. The high spatial frequencies, where instability first shows itself, can be smoothed without loss of intermediate frequencies, and so without the unnecessary loss of detail. With these considerations in mind, trials were performed increasing the order of artificial diffusion from ∇^2 to ∇^4.

Changed convective closure parameters: Convective closure parameters were changed back to "Standard" as used in larger scale models.

∇^4 diffusion and standard convection parameters have a generally beneficial impact on forecasts. ∇^4 diffusion has the expected effect of sharpening features such as troughs and convergence zones. This has a very minor impact on winds (as gradients tend to be increased) but the primary effect is on organized precipitation areas, which tend to be more active features. Small amounts of additional cloud are also produced, especially at medium level.

The use of standard convection parameters has an impact on the precipitation and also tends to produce more low cloud. Not surprisingly, the most important impact is on shower activity, which is often reduced in extent and generally is represented more realistically.

The combination of ∇^4 diffusion and standard convection parameters has quite a marked impact on precipitation. For example, in the 23/8/91 case, used as part of the original MM trial, the rainbands associated with the depression moving up the Irish Sea (Fig. 1) are better resolved and generally handled more realistically, particularly as the forecast develops. The low is also a little deeper, a common feature of ∇^4 diffusion forecasts. Shower activity tends to be (beneficially) reduced, and structure in the shower activity better resolved. In another example (fig. 2), on the 12th April 1993, the Limited Area Model (which provides initial and boundary conditions for the MM) produced showers more or less uniformly over the whole UK around midday. The operational MM did not add much to this: it produced widespread showers over much of England and Wales, and failed to reproduce a gap in the shower activity over central eastern England and Wales. The change to ∇^4 diffusion and standard convection parameters improves the forecast considerably. At 12Z the shower distribution is much more realistic, with the correct location of showers over England.

Convection increments only updated every alternate timestep: This is purely to reduce the CPU time required by the model, and has been found to reduce average by about 10% with negligible impact on the forecast.

Automatic MOPS: The MM Moisture Observation Preprocessing System (MOPS) developed out of the cloud analysis part of the OMM Interactive Mesoscale Initialization (IMI), and relied on forecaster intervention to correct gross errors in cloud top height and cover. These were particularly likely when the inversion associated with the top of a stratocumulus sheet was poorly resolved in the model. This system has been replaced with a fully automated system which uses new algorithms. The aim is primarily to remove the forecaster time required, although it is possible that a more statistically uniform analysis may result. Trial results show that although the analysis may be different from that produced interactively, the impact on the forecast is small but generally beneficial. The system has been operational since October 1993 without any noticeable degradation in the operational forecasts.

"Frozen Physics": Changes were made in line with improvements to larger scale configurations, comprising

1) Removal of the assumption of random overlap of cloud in long wave radiation scheme.
2) An improved numerical treatment of the non-local turbulent mixing scheme in the boundary layer, Geleyn surface layer interpolation and internally consistent surface layer treatment.
3) A fully divergent parametrization for ice in the precipitation scheme and different threshold liquid water contents for precipitation formation over the land and sea (8×10^{-4} and 2×10^{-4} kg m^{-3} respectively).

Fog and Low Cloud: The following changes were all made to improve the treatment of fog and low cloud.

- New fog and cloud diagnostics.
- Revised assimilation parameters
- Screen level relative humidity (RH) assimilation
- Increased vertical resolution.
- Revised critical RH profile.

The new fog diagnostic is presented as the probability of observing visibility at a point at screen level. It is intended to take account of the potential patchiness of fog, which, if ignored, can lead to patchy fog being interpreted as widespread mist. It is (currently) derived in a very simple way consistent with the sub-gridscale parametrization of cloud and RH. The low cloud diagnostic is intended to have a similar purpose, giving the probability of finding cloud below 1000 ft above sea level. It is derived from the forecast cloud fraction below 1000 ft.

The assimilation of screen level RH is probably the single most important change to influence fog forecasting, at least in the first 12 hours of a forecast. The impact is, of course, variable but is illustrated by a case on 30/04/93. The area of fog formation on 30/04/93 is well illustrated by Fig. 3, which shows a sequence of visible METEOSAT images from 06Z to 12Z together with a summary of surface observations from 03Z to 12Z. The images have been enhanced to show the low cloud more clearly. This shows that the fog was still becoming established at 03Z (it had been absent at 00Z, the model analysis time), while by 09Z it was beginning to lift into stratus at the edges. The area of low cloud or fog covering much of eastern England gradually cleared until by 13Z only a couple of thin patches are visible. It is particularly interesting that to the north of England the fog is bounded by the Pennines and does not extend over the North Yorkshire Moors. A strip of thin fog extends up the east coast as far as the Firth of Forth, where, on the earlier frames, it extends inland. Although on the original imagery it is evident that this coastal fog is thinner than that over land, it was much more persistent, lasting through most of the day.

Fig. 4 shows fog probability charts from the operational configuration. The sea fog off the north east, and its encroachment into land, are quite well handled. The fog over Ireland gives a useful indication but is rather underdone. Over England, the fog probability gives a hint of fog in the

right areas at 03Z, mainly in the 10-30 % range, and probably represents a useful if underdone forecast. However, by 06Z the (low probability) fog area has shrunk considerably, and has gone by 09Z. Thus, although the model was trying to form fog in the right areas, by sunrise not enough had formed to prevent the sun burning it off very rapidly. The main reason for this is that the initial conditions from the LAM were too cold and dry.

Without any assimilation (but including ∇^4 diffusion) the model retains many of the features of the LAM run during the night: at 03Z the temperatures are fairly similar, although the fog cleared somewhat from the SW and is controlled more by the MM orography and land-sea mask. By 06Z, temperatures over central England increased to agree fairly well with observations, indicating that the model response to sunrise was quite realistic. Inclusion of assimilation of screen temperature improves the screen temperature at 06Z somewhat further, but that the main improvement in screen temperature comes from the model physics itself. However, warming up to roughly the correct temperature prevents the formation of fog.

Assimilating screen RH in addition to screen temperature goes quite a long way towards rectifying the problem. Fig. 4 shows the fog probability charts. The 06Z chart shows much more developed fog in very much the right area. The spatial extent is still not enough: the 10% line encloses much, if not all, the fog area but clearly should indicate greater probability. This is reflected in the 09Z chart, which shows much of the fog dissipated.

The lowest level of the MM when made operational was at (approximately) 25m. Thus it is likely that, on occasion, relatively thin radiation fog may not be deep enough to produce enough (if any) liquid water at this level to allow radiative feedback processes
to thicken the fog. Operational constraints and internal consistency of the boundary layer scheme restrict the vertical resolution of the model, but it has been improved by adding a single extra level at (approximately) 10m and adjusting the levels above to maintain a uniform gradation of layer thickness. At the same time the critical RH for cloud formation used in the scheme has been modified to depend on layer thickness. The impact of this and the other physics changes case discussed above on the 30/04/93 are shown in Fig. 4. Clearly, the improvement over the operational case is dramatic.

Future Changes

Many of the problems that arise in mesoscale forecasts are caused by errors in the initial analysis. In particular, the fields resulting from interpolation of the larger scale model output may represent cloud very poorly. In spite of data assimilation the early stages of the forecast thus be deficient in mesoscale detail. It is intended that, from next spring, the Met Office MM will be run in a continuous assimilation mode, with a three hour cycle, so that an analysis will be produced every three hours based on assimilation starting from the previous analysis. Forecasts will be run from the 00Z and 06Z analyses. Trials have shown that, while by no means curing all the problems arising from errors in the initial conditions, this generally has a beneficial effect on the forecast. Fig. 4 shows the impact on the (already much improved) 30/04/93 case. Comparison with the original operational run shows an extremely encouraging improvement.

Beyond this, work has started to add aerosol as a prognostic variable in the model, primarily as an aid to visibility forecasting.

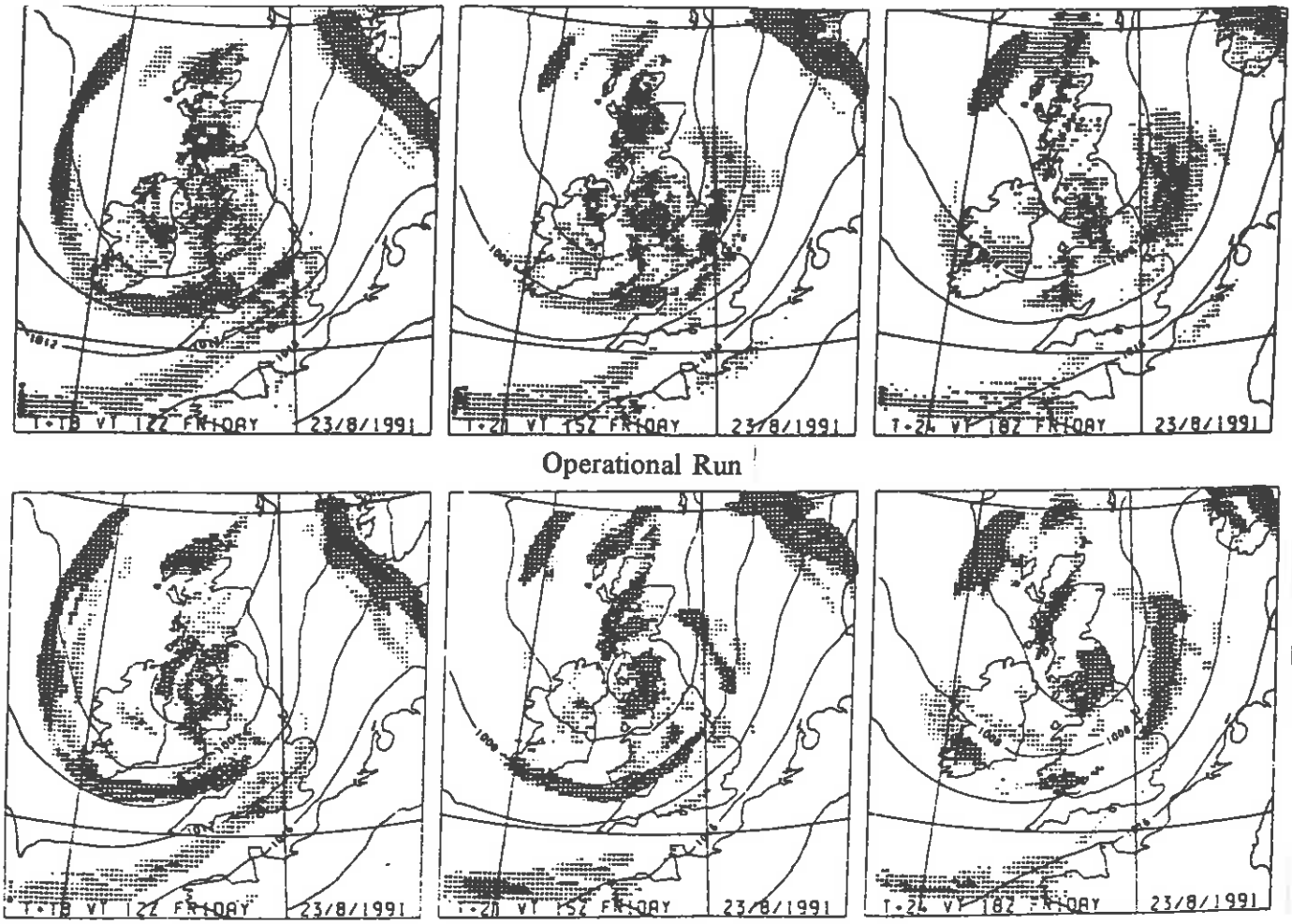

Fig. 1 Comparison of Operational Configuration with ∇^4 and Standard Convection Parameters, 23/8/91

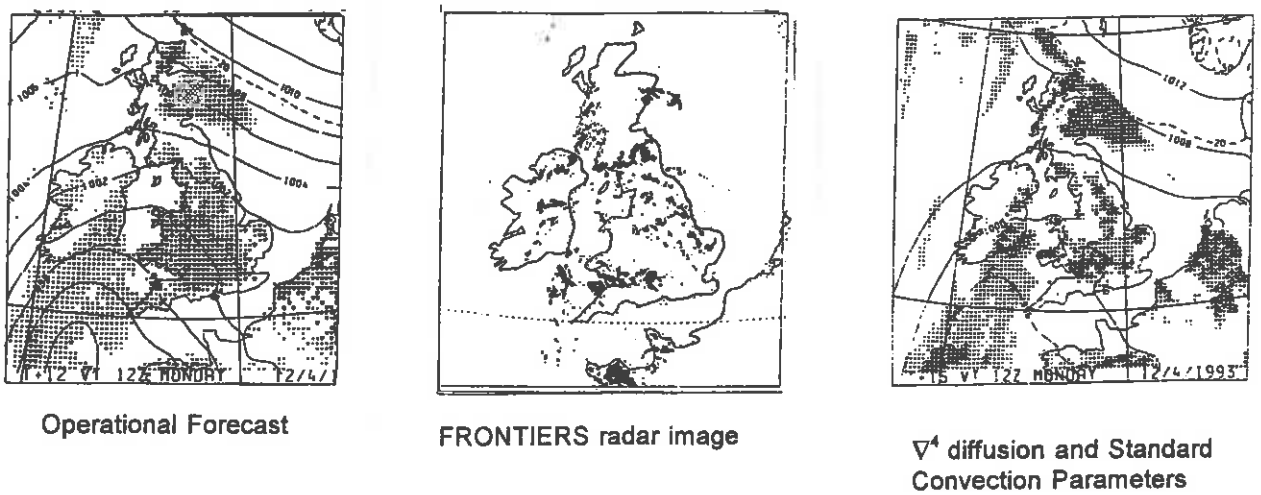

Fig. 2 Comparison of Operational Configuration with ∇^4 and Standard Convection Parameters, 12Z (T+12) 12/4/93

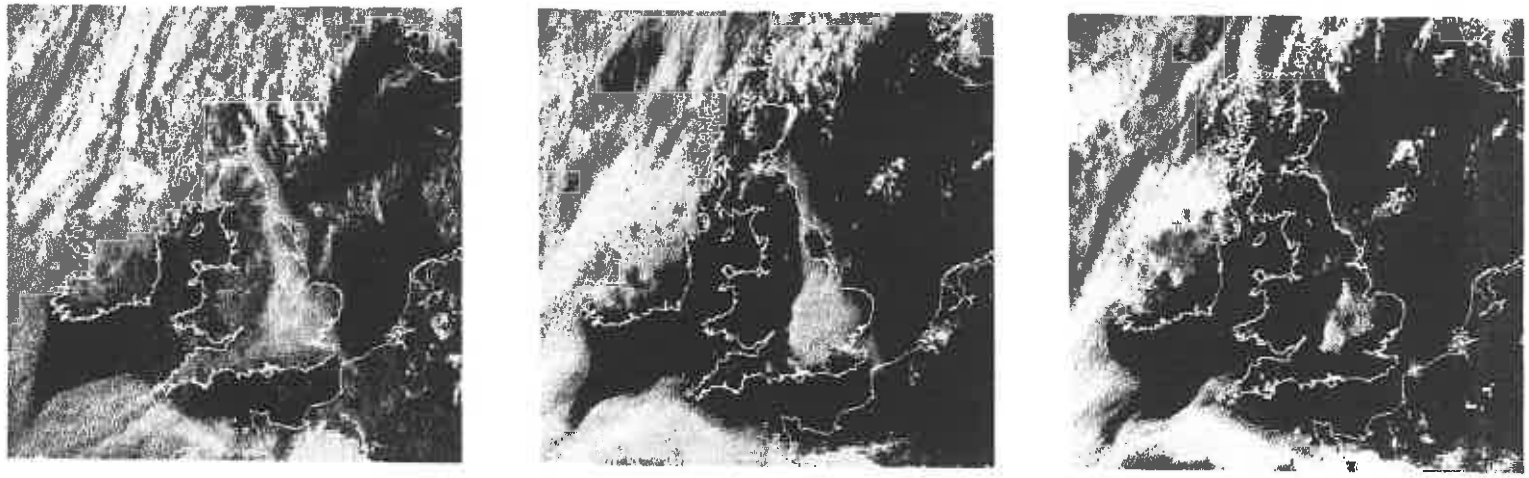

06Z 09Z 12Z

03Z 06Z 09Z

Fig. 3 Visible METEOSAT Imagery and Summary of Surface Observations, 30/04/93

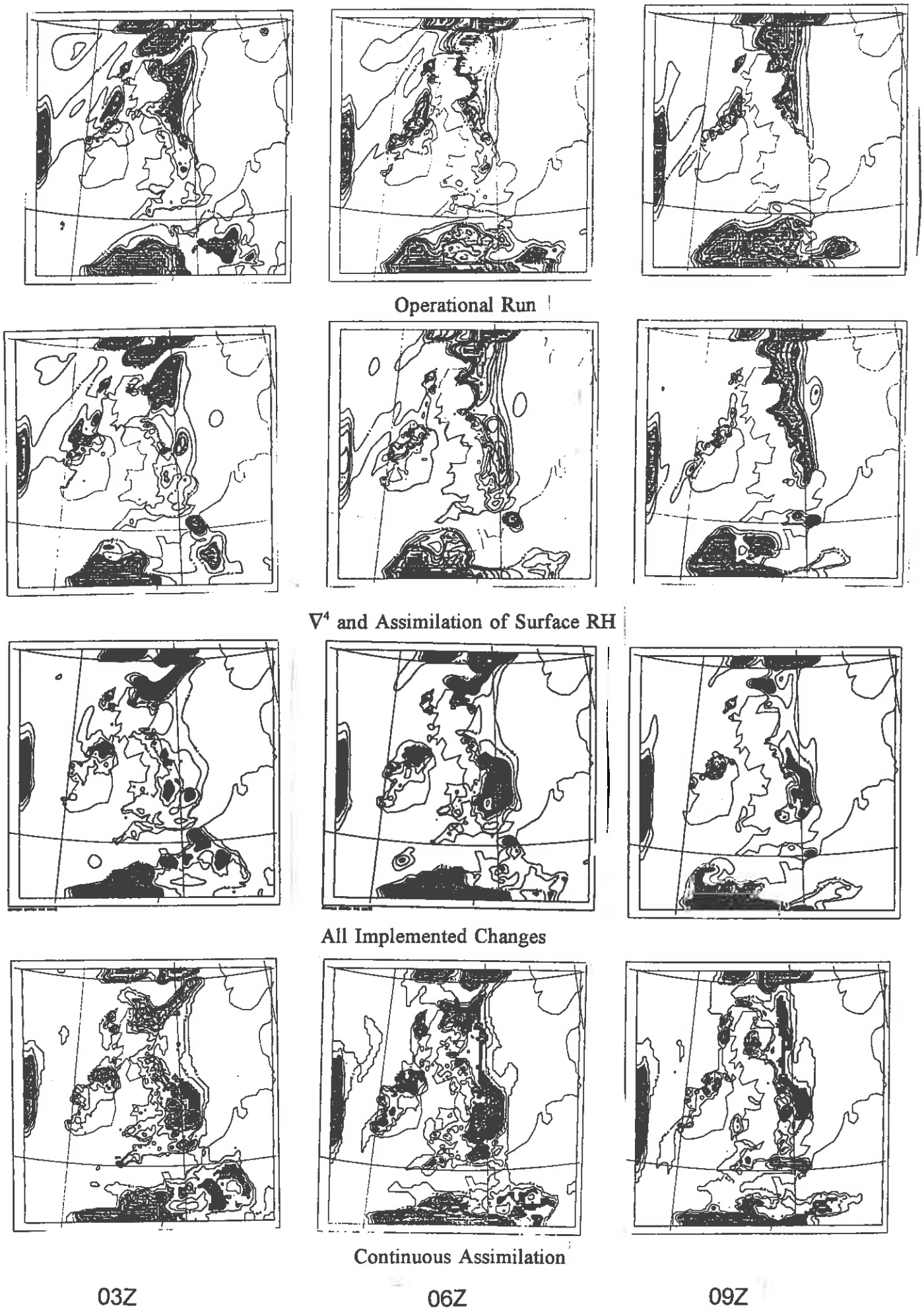

Fig. 4 Comparison of Fog Forecast by Different Model Configurations, DT 00Z 30/4/93

Use and Development of the Unified Model for Case Study Investigations and Improvement of the Prediction of Cloud and Precipitation.

S.P.Ballard, M.G.Hutchinson and C.S.A.Davitt

Met Office Unit, Joint Centre for Mesoscale Meteorology,
Harry Pitt Building, Univeristy of Reading,
Whiteknights Road, PO Box 240, Reading, RG6 2FN, UK
email:spballard@email.meto.govt.uk

1. Introduction

As part of the expansion of the JCMM in 1992 a new group was formed with the aim of undertaking research to improve the prediction of cloud and precipitation in the unified model and investigate mesoscale predictability. Part of the aim was to draw upon the work of other groups in the JCMM involved in field study investigations and cloud scale modelling.Some of this work is summarised below or described in reports in the reference list. Any scientists interested in working at the JCMM under the Met Office visiting scientist programme should contact Sue Ballard at the above address.

2. Development of new cloud and precipitation scheme for the Unified Model including explicit prediction of ice/snow.

One of the requirements for the operational versions of the unified model is to provide forecasts of the likelihood of helicopter icing due to flying through supercooled liquid water. It is also important to be able to accurately predict the phase of surface precipitation due to the impact of snow on surface and air transport etc.

In the current grid-scale/stratiform cloud scheme used in the unified model (Smith 1990) both liquid and frozen cloud water are assumed to condense/freeze and evaporate/sublimate instantaneously once air becomes super- or sub-saturated. Partial cloud is treated assuming sub-gridscale distributions of temperature and humidity cf Sommeria and Deardorff (1977). All cloud is formed as ice as soon as the temperature drops below freezing. For the purposes of radiation calculations and production of precipitation, mixed phase cloud is allowed for by repartitioning the diagnosed cloud ice between ice and liquid water using a quadratic function of temperature between 0°C and -15°C. Precipitation at the surface can only be snow if the lowest model level temperature is at or below freezing.

A new scheme is being developed to allow the explicit prediction of ice and mixed phase cloud and precipitation. This is initially based on the scheme implemented in the non-hydrostatic model (Golding 1992,1993, and Marecal et al 1994) but is being modified to allow its use at coarser resolution and longer time-steps, and to include more general formulations of the microphysical exchange terms.

3. Investigations of the prediction by the unified model of the humidity, cloud and precipitation associated with a developing frontal wave observed during FRONTS 92.

During spring 1992 an observational field programme was carried out by the JCMM to investigate the mesoscale structure of frontal waves (Hewson 1993). IOP3 on 27/4/92 has

been selected for intensive study. 63 Dropsondes measuring wind, temperature and humidity were deployed from the MRF Hercules in the vicinity of a developing cold front wave in the SW approaches to the UK between 12UTC to 21UTC 27/4/92 which was coincidentally the period during which it underwent its most rapid development. The low tracked east-north- east through the English Channel during the night 27-28/4/92 producing many hours of rain over southern England. Additional measurements were obtained from radiosondes launched from Larkhill between 13UTC 27/4/92 and 13UTC 28/4/92 and the Chilbolton dopplerised dual polarisation radar in southern England. These supplemented routine, synoptic, satellite and radar data.

The wave was first identified on 25 April 1992, as a slow moving feature about 1000km south-east of Newfoundland. The wave accelerated in an easterly direction with little or no development before deepening 12mb in 12 hours after 12UTC 27 April. Two cloud masses stayed attached to the system after 12UTC 26, a northern 'cloud head', which developed in situ, and a southern frontal cloud band. Water vapour imagery showed a region of dry air which intruded into the wave around 00UTC 27. It developed a double structure, the southern portion winding round the cloud head and over the low centre. Preliminary analysis by Browning et al (personal communication) indicates that these two dry intrusions were associated with two surface cold fronts trailing southwestwards from the tip of the cloud head, the easternmost evolving into an upper cold front as the dry air overran the surface front and triggered mid-level convection near the low centre where it began to overrun the warm frontal zone. These showers weakened from 22UTC 27 onwards. The main rain area was associated with the cloud head region. From the drop-sonde data and satellite imagery, fine-scale structure was evident within the dry intrusions in the form of multiple dry/moist laminae near the top of the boundary layer with vertical wavelength 1km and slope of 1 in 100. At 06UTC 28 the broad-scale structure of the system was similar to that described in Browning and Roberts 1993. Surface synoptic observations indicated a frontal fracture between the cloud head and cold front 2. Chilbolton radar scans and satellite imagery indicated mid-level convection aligned along the bend of the cloud head in the upper part of the region of slantwise ascent within the cloud head.

The ability of the Unified Model to predict the mesoscale structure associated with the developing frontal wave in IOP3 of FRONTS 92 is being investigated.

The sensitivity of predictions using the operational configurations of the UK Met Office Unified Model model at 90,50 and 17km resolution to initial conditions, data assimilation, resolution and model formulation have been investigated so far. Longer range forecasts (30 to 48 hours) showed the advantage of higher resolution in correctly simulating the intrusion of dry air into the centre of the developing low, although improvements in the coarser resolution forecasts were obtained from changes in model formulation, such as reduced diffusion of moisture.

Allowing for its limited resolution, the operational global version of the unified model provided consistent and accurate 4 to 2 day forecasts of the development and positioning of the IOP3 low. Unfortunately the shorter range forecasts of both the global and limited area models were less reliable with a tendency to take the low slightly too far south, not to deepen it sufficiently before it reached the English Channel and not to fill it sufficiently when it reached the northern French coast. The Limited area model analyses did not capture the details of the distribution of cloud, humidity and precipitation shown by the satellite, dropsonde,

radiosonde and radar data. In particular the intrusion of dry air into the centre of the system was underdone as was the intensity of the precipitation associated with the cloud head. However, despite some errors in the development and positioning of the low, the LAM forecasts did capture many of the details of the observed system. In particular the double structure in the dry air and the intrusion of dry air into the centre of the system. This was particularly true of the 12UTC 26/4/92 forecast. Shorter range forecasts with less development of the low had a tendency for insufficient over-running, or erroneous moistening, of the dry air and this is being investigated.

In order to improve the LAM analyses and to allow maximum benefit from assimilation of drop-sonde data a continous LAM assimilation was run from 00UTC 26/4/92 to 12UTC 28/4/92 with the latest operational version of the model and using the global model assimilation as boundary conditions. Benefit was obtained from continous assimilation of the operational observations at high resolution as opposed to only a 6 or 12 hour spin-up from a global model analysis in the definition of the precipitation and humidity fields. The humidity, in particular the definition of the dry intrusion , and precipitation analyses were greatly improved by the inclusion of the drop-sonde data as were forecasts from 18UTC 27/4/92, see figures 1 and 2.

Mesoscale forecasts from 12UTC 26/4/92 and 18UTC 27/4/92, see figures 1 and 2, provided useful extra resolution of the observed features associated with the wave. The definition of the dry intrusion was improved as well as the distribution of precipitation. At 06UTC 28 the frontal fracture was well represented as well as mid-level convection in the region of slantwise ascent in the cloud head. It is planned to run a continuous mesoscale assimilation from 00UTC 27/4/92 to 12UTC 28/4/92 and include the drop-sonde data to provide further insight into the representation of the observed fine-scale processes and the requirement for improvements to the model formulation.

4. Investigations of the prediction of a front interacting with the Alps- May 3rd 1987- by the ECMWF and Unified Models.

The unified model at global, LAM and mesoscale resolutions was run from an ECMWF analysis for 12UTC 2nd May 1987 to investigate the prediction of a front interacting with the Alps as input for the Meteorological Office/Reading University Summer School on orographic processes. The skill was limited due to initiation from coarse resolution data however the runs showed the benefits of mesoscale resolution in predicting observed features such as a pressure surge to the north of the Alps, see figure 3, and a strong orographic jet.

5. References

Ballard,S.P.,Jackson,S. and Macpherson,B. 1993 'Short-range forecasting of Stratocumulus', proceedings of ECMWF workshop on Parametrisation of the cloud topped boundary layer, 8-11 June 1993.

Ballard,S.P. and Macpherson,B. 1993 'Operational performance of mesoscale and LAM models in prediction of stratocumulus', Forecasting Research Technical Report No 56.

Ballard,S.P.,Robinson,R.,Barnes,R.T.H.,Jackson,S. and Woltering,S. 1993 'Development and performance of the new mesoscale model', Forecasting Research Technical Report No 40.

Browning,K.A. and Roberts,N. 1993 'Structure of a mid-latitude cyclone before occlusion', JCMM Internal Report 5, to appear in Q.J.R.Meteorol.Soc

Golding,B.W. 1992 'An efficient non-hydrostatic forecast model. Meteorol.Atmos.Phys.,50 89-103.

Golding,B.W. 1993 'A numerical investigation of tropical island thunderstorms. Mon Wea Rev., 121 1417-1433.

Grant,J.R.,Bader,M.J.,Wilson,C.A.,Davies,T. and Ballard,S.P. 1993 'The 1992 Autumn Equinoctial Downpour: Causes and NWP model Assessment', Forecasting Research Technical Report No 59.

Hewson,T.D. 1993 'The Fronts 92 experiment: A quicklook atlas', JCMM Internal Report No 15.

Marecal,V., Illingworth,A.J. and Ballard, S.P. 1994 'Observation and modelling of the aggregation process in a frontal rainband', this volume.

Smith,R.N.B. 1990 'A scheme for predicting layer clouds and their water content in general circulation models', Q.J.R.Meteorol. Soc., 116, 435-460.

Sommeria,G. and Deardorff,J.W. 1977,'Subgrid-scale condensation in models of nonprecipitating clouds. J.Atmos.Sci 34 344-355.

Forecasting Research Technical Reports and JCMM Internal Reports can be obtained from the National Meteorological Library, Meteorological Office, London Road, Bracknell, Berkshire, RG12 2SZ, England.

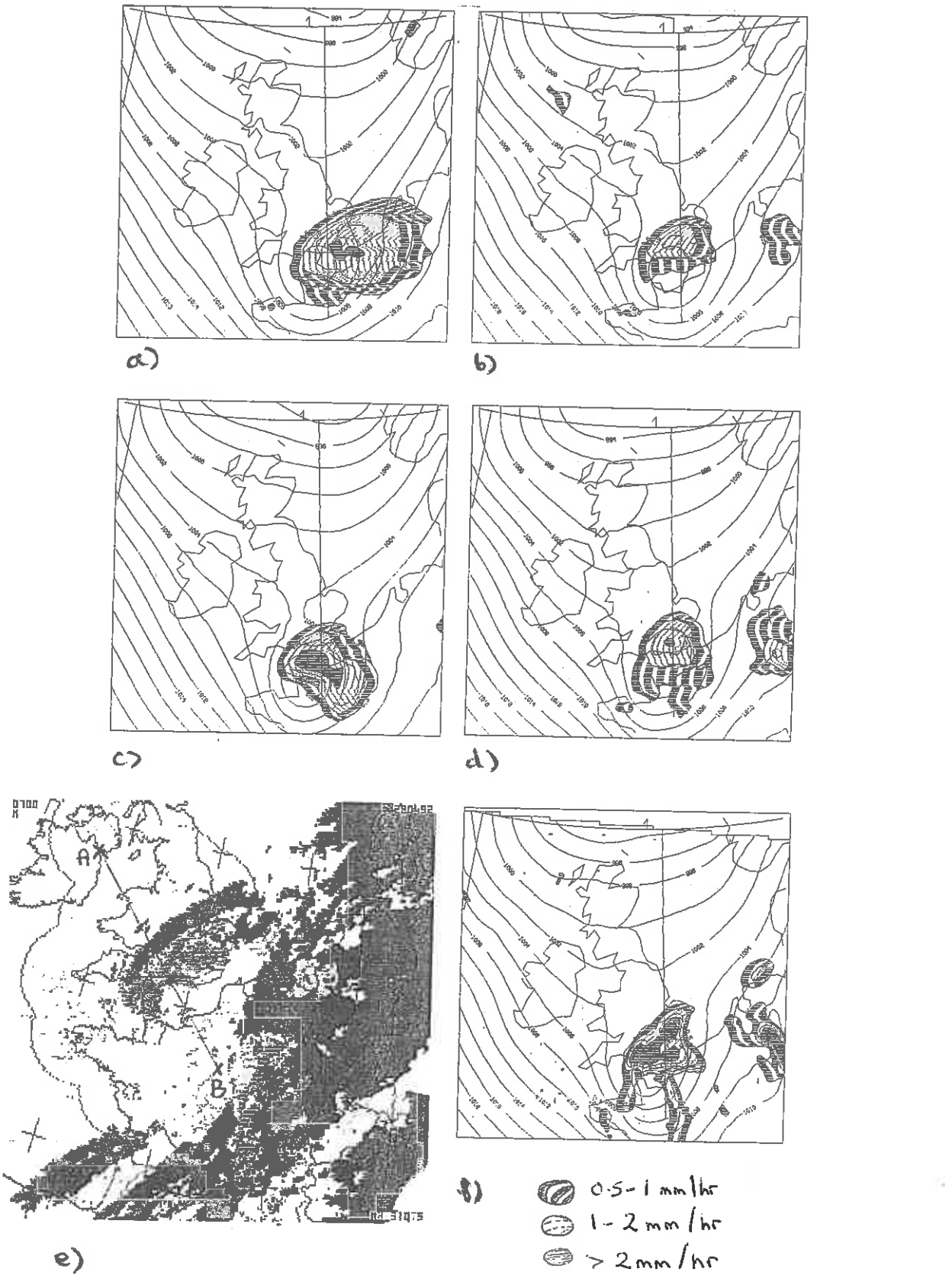

Fig.1 Verification of analysed and forecast surface precipitation rates valid at 06UTC 28/4/92. a) operational LAM analysis, chart shows mean sea level pressure and total precipitation rate, b) as a) but LAM analysis from continuous assimilation cycle starting 00UTC 26/4/92 and including drop-sonde data, c) 12 hour LAM operational forecast from 18UTC 27/4/92, d) 12 hour LAM forecast from 18UTC 27/4/92 analysis taken from continuous assimilation cycle including drop-sonde data, e) COST 72 radar image valid at 07UTC 28/4/92. Lighter shades are radar data, black is area of high cloud from Meteosat IR image, also shown is line of section AB used in fig.2 , f) 12 hour mesoscale forecast from LAM analysis as used in d)

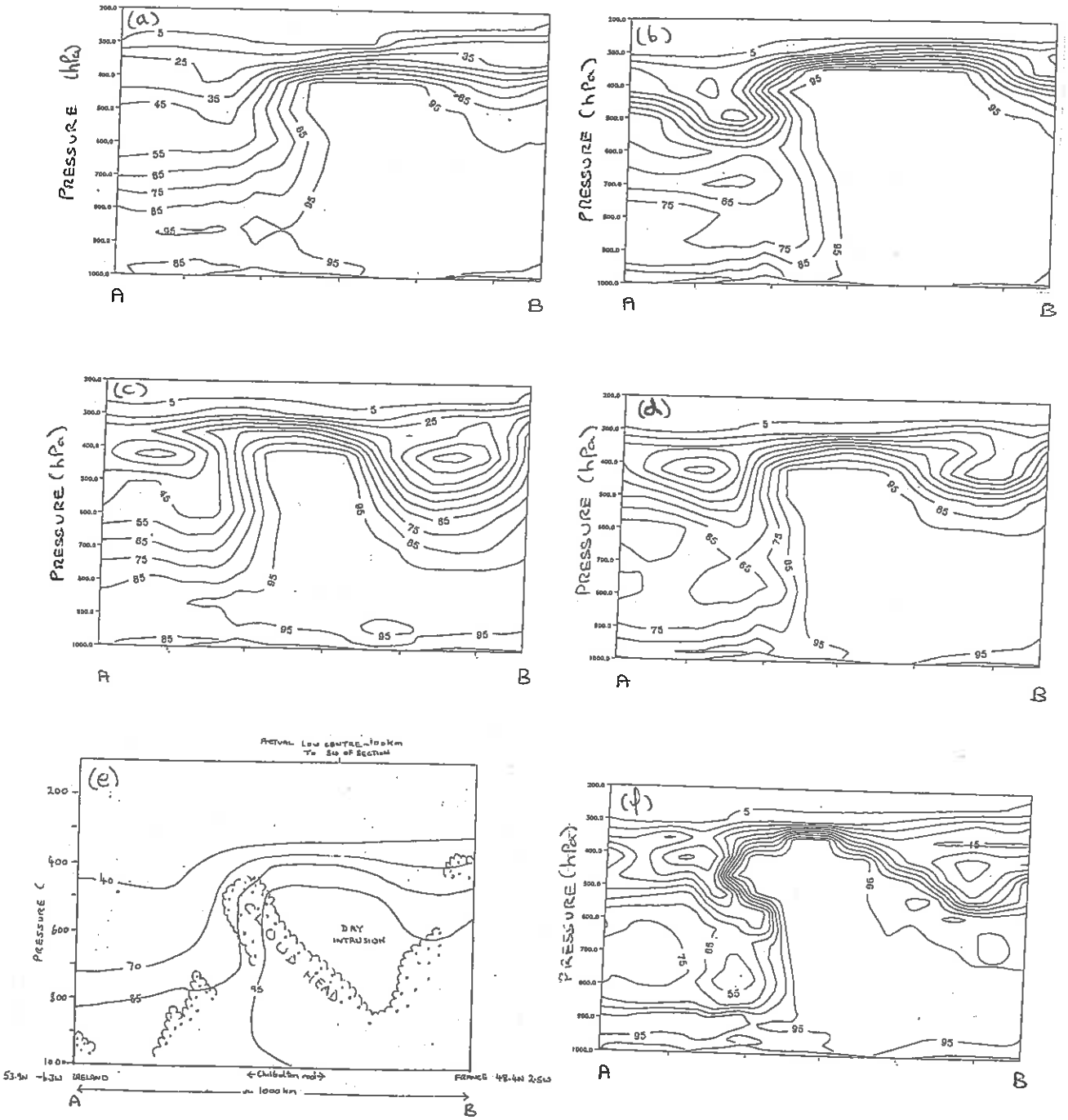

Fig.2 Cross-sections of relative humidity and observed cloud top pressure at 06UTC 28/4/92 along line AB shown in Fig.1. a) operational LAM analysis , b) 12 hour LAM operational forecast from 18UTC 27/4/92, c) LAM analysis from continuous assimilation cycle starting 00UTC 26/4/92 and including drop-sonde data, d) 12 hour LAM forecast from 18UTC 27/4/92 analysis taken from continuous assimilation cycle including drop-sonde data, e) cloud top pressure taken from Meteosat IR image, also shown is smoothed relative humidity from a), f) 12 hour mesoscale forecast from LAM analysis as used in d) .

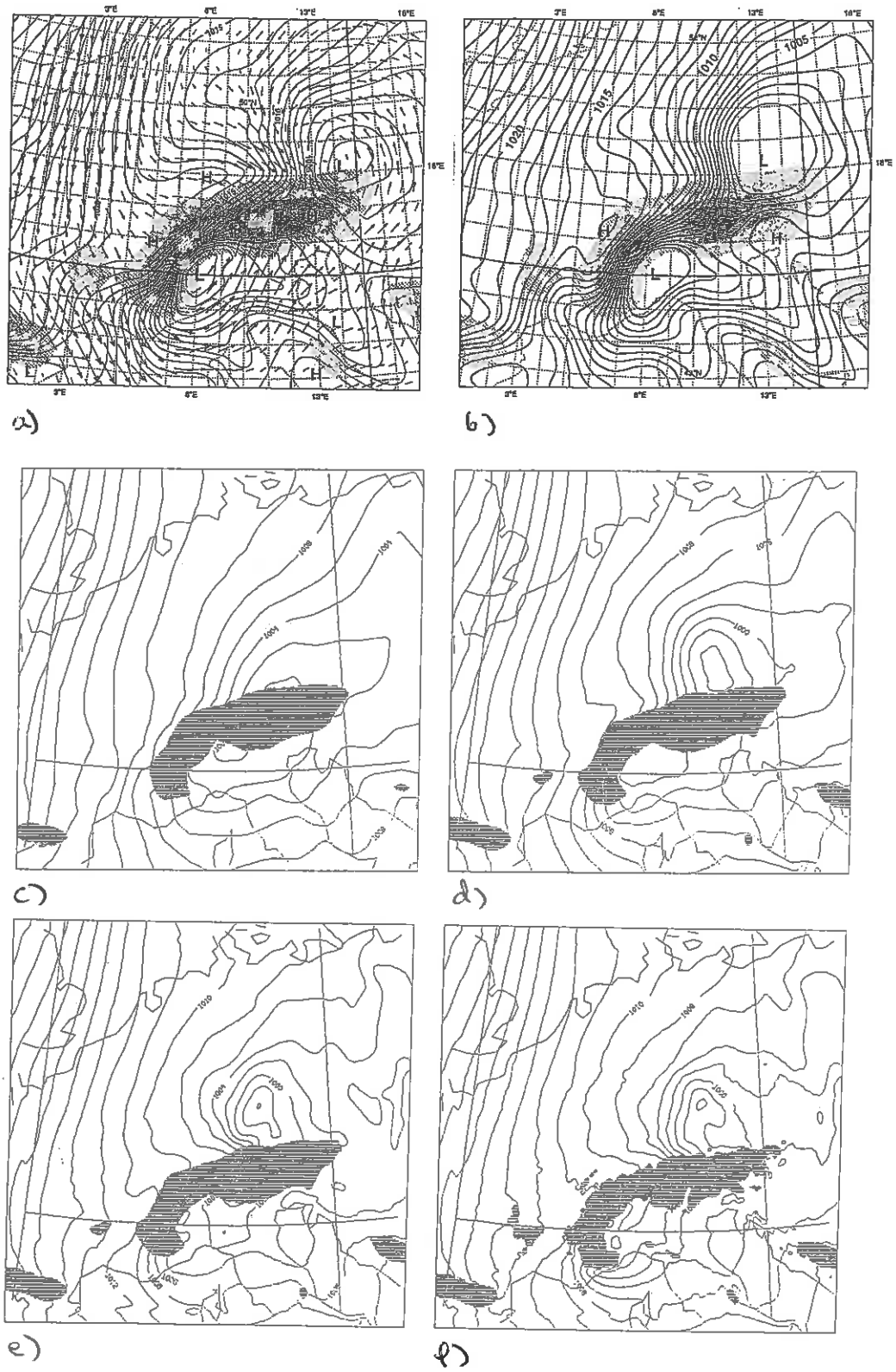

Fig.3 Comparison of analysed and forecast mean sea level pressure valid at 18UTC 3 May 1987. a) ECMWF T213 analysis with 850hPa wind, b) ECMWF T213 forecast from 12UTC 2 May 1987, c) Global unified model (90km) forecast from 12UTC 2 May 1987 ECMWF analysis data, d) as c) but Limited Area Model (50km), e) as c) but mesoscale model (17km) with interpolated LAM orography, f) as e) but orography extracted from 5' data. Isobars every 1 hPa ECMWF, 2hPa UKMO, lat/long lines every 1° ECMWF, 15° UKMO. Model orography shaded above 1000m.

Modelling the Mesoscale Effects of Land Surface Heterogeneity in the Sahel

Christopher Taylor, Richard Harding (Institute of Hydrology), and Alan Thorpe (Joint Centre for Mesoscale Meteorology)

Introduction

The aim of this joint project between the Institute of Hydrology and the Joint Centre of Mesoscale Meteorology is to develop an understanding of the effects of land surface heterogeneity on the atmosphere. The investigation is focused on heterogeneity occurring on length scales of 10's km, which may be expected to generate spatially variable planetary boundary layers (PBL). We hope to improve the representation of these boundary layer processes which occur on sub-grid length scales in GCMs. The work is primarily based around the HAPEX-Sahel experiment of August to October 1992 in south west Niger.

Heterogeneity

The HAPEX-Sahel experimental area (13-14N,2-3E) contains heterogeneous land surfaces on a variety of scales. The terrain is very flat, but contrasts exist due to different land use patterns and sub-surface hydrology. There is also a north-south gradient in the density of vegetation due to the gradient in rainfall on timescales of several years. This indicates the strongly limiting effect of rainfall on the growth of vegetation in this region. In addition, at any particular time during the wet season, there is strong heterogeneity in the near-surface soil moisture. This is due to highly localised rainfall patterns, and can generate strong contrasts in evaporation on length scales of the order of 1km up to perhaps 100km. Fig (1) shows the total rainfall measured by the rain gauge network for the month of August 1992.

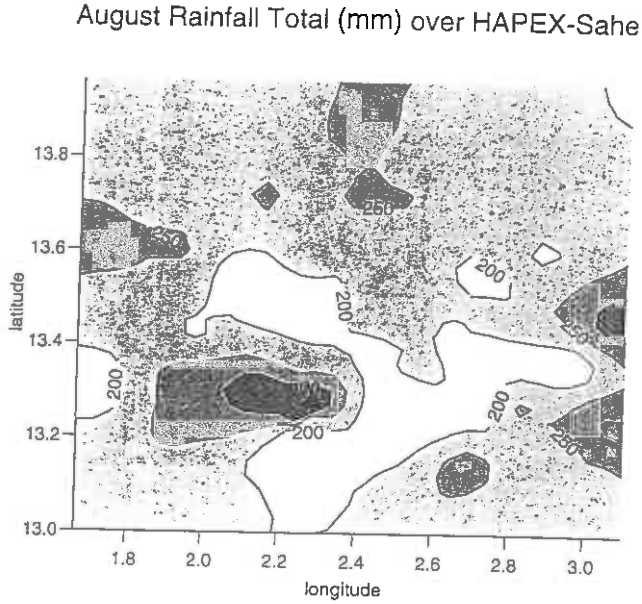

Figure 1 Total rainfall for August 1992 for the HAPEX-Sahel square.

Work is in progress on producing fields of surface parameters for the region around the HAPEX-Sahel square. This involves

(a) preparing a land use map from remote sensing (AVHRR) for vegetation parameters
(b) digitising a soil classification map for soil parameters
(c) running a simple soil moisture model over the wet season to initialise the soil moisture fields. The model takes inputs of daily rainfall calculated from cold cloud-top temperatures collected by the TAMSAT group at Reading University.

Mesoscale Model

For this project we are making use of the Meteorological Office Unified Mesoscale Model. This has been set up to run on the Cray at the Rutherford Appleton Lab. The model is used to simulate the development of the planetary boundary layer above resolved heterogeneity (0.15°) in land surface parameters.

Several 24 hour simulations have been run from 00:00 on the 8th October 1992. This was a day free from cloud over much of the domain, several weeks after the last major rainfall event. The simulations are initialised with an operational analysis from the Met.Office global forecast model. Without the realistic higher resolution surface maps currently being prepared, the surface parameter fields from the global model (resolution 1.25° longitude, 0.83° latitude) are interpolated onto the mesoscale domain.

In the case of soil moisture, a climatological map is used in the global forecast model which captures the north-south gradient in rainfall in only a very coarse way. In particular, high values of soil moisture are assigned to areas some 450km to the north east of the HAPEX square. Over the HAPEX square, the climatological soil moisture is considerably lower than observed.

Model Results

In the model, the soil moisture deficit modifies evaporation from the surface by a factor β, which lies between 0 and 1. Fig.2(a) shows how this factor varies over the entire domain. In the north of the domain, soil moisture is close to zero, resulting in low latent heat fluxes and high sensible heat fluxes. By 16:00 in the simulation, the boundary layer has deepened to over 2500m in places (Fig.2(b)). This is in contrast to areas in the centre of the domain, where β is close to 1, sensible heat fluxes are low, and the inversion height is less than 1km. A comparison between Figs.2(a) and (b) suggests that over much of the domain, the initial soil moisture field is the principal factor in the development of the boundary layer.

To investigate the effects of soil moisture heterogeneity on the boundary layer, a hypothetical soil moisture distribution was introduced into the model. The soil moisture from one grid point of the global model was redistributed on the mesoscale as in Fig.3, rather than simply interpolated. This was done in such a way as to maintain the same value of β (0.25) when averaged over the area representing one

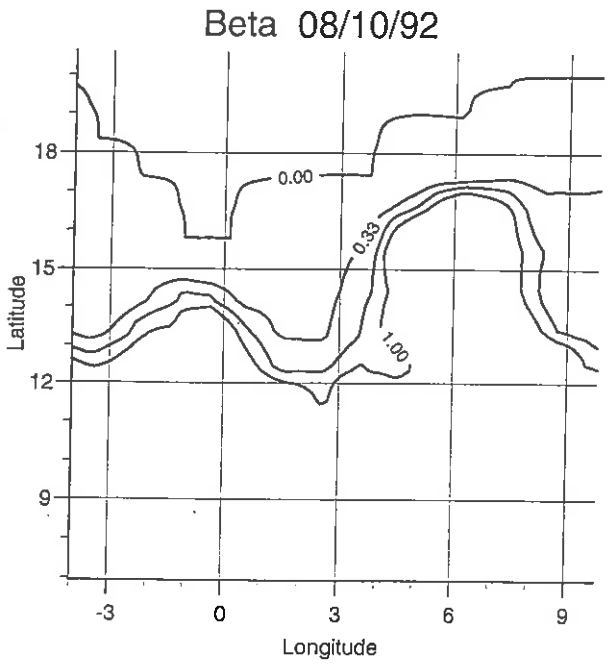

Figure 2a Variation of B - the evaporation factor - over the mesoscale model domain

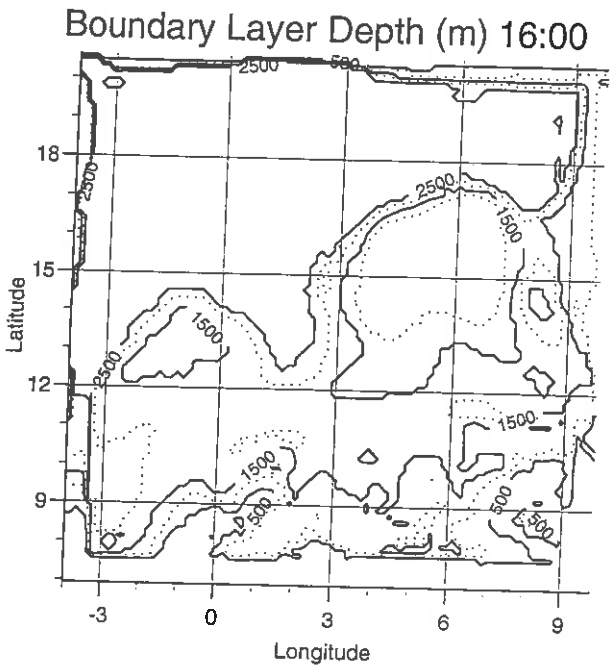

Figure 2b Variation of boundary layer depth as predicted by the mesoscale model for 1600 8 October 1992.

global model grid box. In this case, over some mesoscale grid points β was exactly 1 and elsewhere β=0. Looking at properties of the atmosphere averaged over this GCM grid box, this extreme heterogeneity can reveal the extent of the effects of processes occurring on the sub-GCM scale. Here we focus on the changes induced by the surface on the boundary layer humidity.

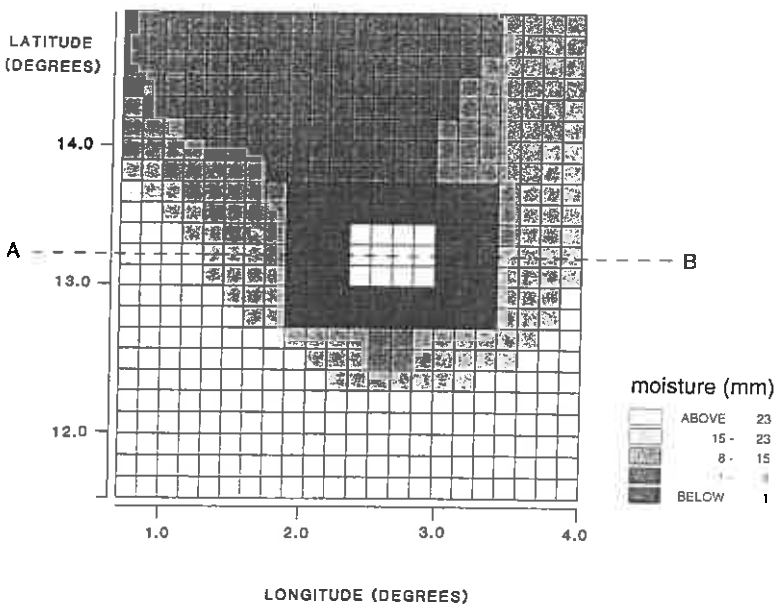

Figure 3 Hypothetical soil moisture distribution used in the mesoscale model run, the line AB corresponds to cross-section shown in Figure 7.

Fig.4 shows the difference in area-averaged specific humidity in the boundary layer between this heterogeneous (oasis) experiment and the original interpolated soil moisture run. This represents the effect of the heterogeneity in soil moisture on the humidity at the GCM scale. There are several features to note from this graph:

(a) throughout the morning the oasis experiment produces a drier boundary layer, averaged over the entire global model grid, at low levels.

(b) around midday, the heterogeneous surface moistens the atmosphere at heights of around 2.5km.

(c) throughout the afternoon, the boundary layer moistens at most levels above the oasis relative to the interpolated soil moisture field.

(d) Moistening due to the heterogeneity is particularly strong at around 2km during the last hours of daylight.

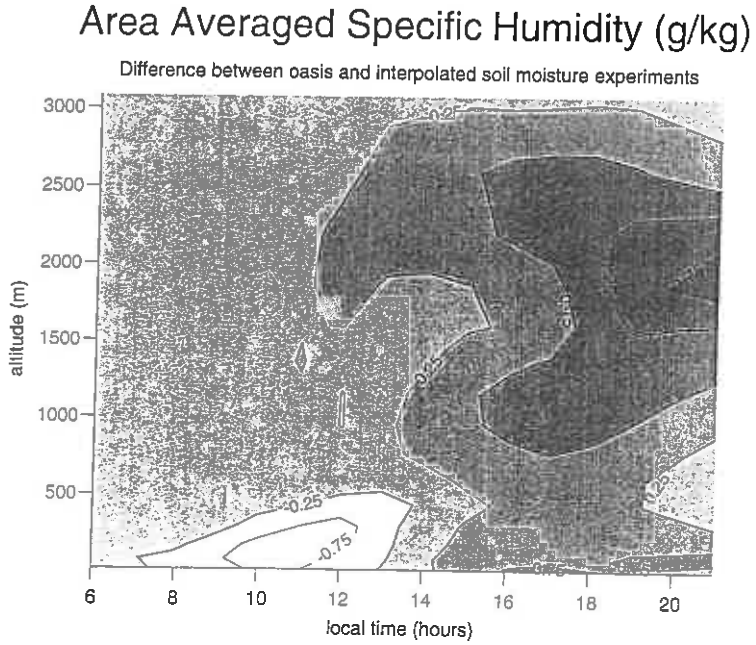

Figure 4 Area-averaged specific humidity, the difference between the heterogeneous experiment and the original smoothed runs.

The area averaged latent heat flux from the two experiments through the day is shown in Fig.5. The heterogeneous surface evaporates at about half the rate of the interpolated surface, leading to the drying at low levels noted in (a). This is due principally to the difference in temperatures of the wet oasis surface and the moderately wet interpolated surface. A simple analytical model based on the Penman-Monteith equation can be used to estimate the effect on area-averaged evaporation of this heterogeneity. The ratio of the evaporation from the heterogeneous and homogeneous surfaces are plotted in Fig.6. as a function of

temperature in the boundary layer. This predicts that at high temperatures and low values of β, area-averaged evaporation can be reduced by up to a half with this type of heterogeneity. Boundary layer feedbacks on the surface fluxes are relatively small in such situations. This suggests that in terms of representing the surface fluxes at the GCM scale, a "tile" model such as that developed by Avissar and Pielke (1989) for heterogeneous vegetation is reasonable. This couples two surface energy balances, one wet and one dry, with the same area-averaged boundary layer variables.

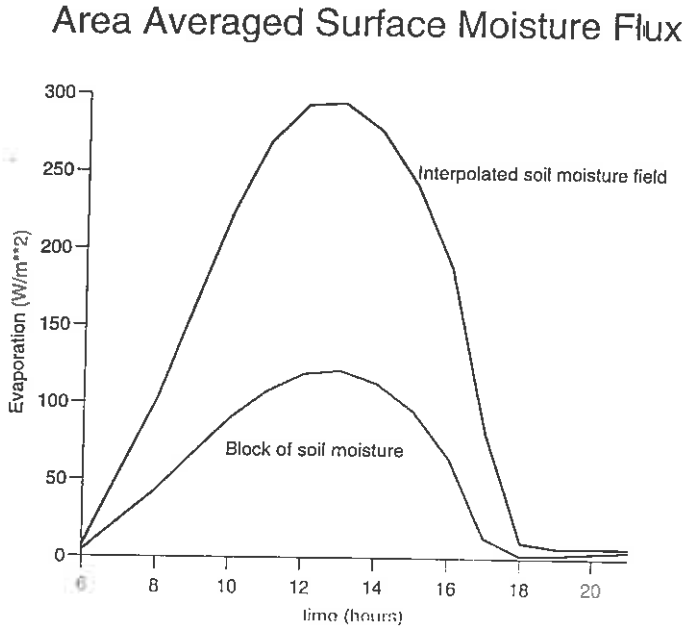

Figure 5 Area-averaged latent heat flux calculated with heterogeneous soil moisture (the block) and the original interpolated field.

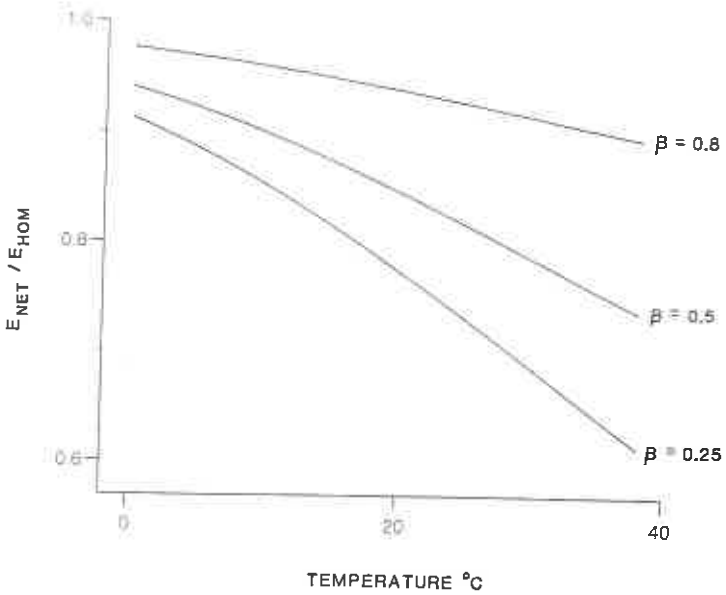

Figure 6 Ratio of evaporation calculated with heterogeneous and homogeneous soil moisture fields as a function of temperature.

The enhanced moistening around midday due to the heterogeneous surface can be understood in terms of variability in the boundary layer above the oasis. Over the wet area, the inversion height remains less than 1km throughout the day. However, over the dry areas, the large surface sensible heat fluxes deepen the boundary layer to up to 3km. In these areas then, turbulent sub-grid scale fluxes transport humidity at low levels up to the much drier regions aloft. In contrast, above the interpolated soil moisture field, the range of boundary layer heights is much smaller. Typically, the height of the inversion occurs at about 1600m. This reduces the vertical fluxes of humidity at higher levels relative to the oasis experiment and leads to the moistening noted in (b).

The heterogeneous soil moisture field introduces high spatial variability into the surface sensible heat flux. Fig.7 illustrates how this generates "sea-breeze" effects imposed on the synoptic easterly flow. This introduces further differences between the two experiments. The resolved mesoscale circulations generate large horizontal and vertical fluxes of humidity in the boundary layer. This is evident from the variability in humidity plotted in Fig.7. Considerable low-level horizontal moisture convergence is nearly balanced by vertical divergence. This produces the gradual moistening at low levels during the afternoon evident from Fig.4. The converse is true at higher levels, with large vertical convergence outweighing horizontal outflow. This effect peaks in late afternoon. The area-average humidity is increased by about 2g/kg at 2km by 21:00. This is in spite of the greatly reduced supply of moisture at the surface already noted.

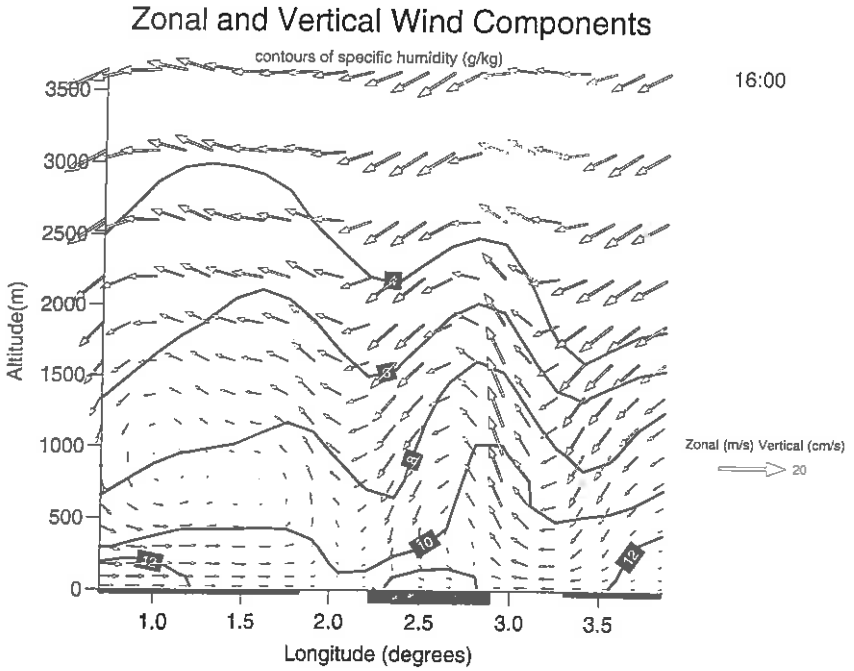

Figure 7 A vertical crossection of the mesoscale model output across a line of constant latitude showing atmospheric humidity, vertical and zonal winds (note the vertical scale is exaggerated) and the imposed, hypothetical soil moisture distribution.

Summary and future work

The mesoscale simulations have demonstrated the importance of soil moisture in Sahellian boundary layer development. This emphasises the importance of a realistic soil moisture map for modelling case studies from the HAPEX-Sahel experiment. The highly localised nature of the rainfall in the region suggests a mechanism for producing highly heterogeneous surfaces on the mesoscale. In such cases, resolved mesoscale fluxes can be at least as important as parameterised turbulent fluxes in the transport of moisture.

It is unclear at present exactly how widespread these land surface-induced mesoscale fluxes may be, and of their relevance to GCMs (eg Avissar and Chen, 1993). This will be in part tackled by investigating the mesoscale model for a range of situations occurring during the HAPEX-Sahel experiment and applying the model in a contrasting climate. Also work will proceed on producing realistic lower boundary conditions when these are available verification will be possible with measured surface and boundary layer fluxes. Finally the question of how to parameterise the mesoscale fluxes in larger scale models remains to be answered.

References

Avissar, R. and R.A. Pielke, 1989: A parameterisation of heterogeneous land surface for atmospheric numerical models and it's impact on regional meteorology. Mon. Wea. Rev. 117, 2113-2136.

Avissar, R. and F. Chen, 1993: Development and analysis of prognostic equations for mesoscale kinetic energy and mesoscale (subgrid scale) fluxes for large-scale atmospheric models. J. of Atmos. Sci., 50, 3751-3774.

New integration scheme for the Met Office Unified Model

M.J.P.Cullen and T.Davies

The current unified model integration scheme uses a quasi-hydrostatic form of the equations of motion and a split-explicit time integration scheme, Cullen et al. (1992). The variables are arranged in the horizontal on a 'B' grid, in which both horizontal velocity components are held at the same point, but are staggered from the temperature and pressure values. This is the only grid arrangement which has been used successfully with the split-explicit method. The method is very efficient in computer time. Within it, it is relatively easy to incorporate different advection and diffusion schemes. Only slight sensitivity of the model to changes in the advection scheme has been found to date, except to the vertical advection of potential temperature which can have a large (20K) impact on tropospheric mean temperatures. There is considerable sensitivity of tropospheric mean temperature and moisture values to the diffusion formulation. The scheme was chosen as the only one which had been demonstrated to work and was acceptably efficient and conservative at the time of the collapse of ETA systems. The unified model project then became very urgent and no further choices could be investigated. The original proposal had been to use the 'C' grid in the horizontal. On this grid the two velocity components are held at different points. However, it proved impossible to get this scheme to work with the split-explicit method. (It is the standard scheme to use with semi-implicit methods). Experience at GLA is that their simulations on the 'C' grid are better than those on the 'A' grid. It is now important to try and develop all aspects of the unified model further. There are some problems with the current unified model clearly attributable to the integration scheme, for instance time traces show oscillations on the scale of two advection or 6 adjustment steps and there are oscillations in vertical wind profiles. Other centres pay much more attention to the dynamical balance of their initial data. Most (e.g. ECMWF) use normal mode initialisation. NMC have removed the need for this by careful calculation of analysis increments. Improving the balance in the unified model is a strong candidate for improving the verification scores, and improving data retention and hence short range forecasts. There is also a clear requirement to be able to run the model at a much higher resolution in the future. The highest current operational resolution is 15km. However, experiments with grids of 2km or less will be necessary at some stage. This will require the ability to run a non-hydrostatic model. Experience with these models is that semi-implicit time integration is required; and that this requires a grid stencil in which the equation solved for the pressure corrections is represented by the most compact possible stencil. We therefore recommend that we move towards a semi-implicit method. This will bring us closer to the common practice in other centres.

2. Proposed integration scheme.

This section describes and justifies the choices made. The full details of the proposals are available on request. A review

has been carried out of the vertical coordinate to be used in a non-hydrostatic model, White and James (1991). This suggests that the coordinate should be physical height, other choices leading to unnecessary approximations. The work involved in changing to height is no greater than that involved in using reference or hydrostatic pressure as the coordinate (Dudhia (1991), Laprise (1992)). The old Meteorological Office mesoscale model used height above ground as the vertical coordinate, Golding (1992). This gave the advantage of a terrain following coordinate and a constant coefficient equation to be solved in the semi-implicit time integration. However, it was believed to lead to unnecessary finite differencing errors in the free atmosphere caused by the sloping coordinate surfaces. James (1992) has developed a method of optimising the vertical grid to flatten the coordinate surfaces above the ground while minimising grid distortion. This is an extension of the method used by Clark (1977). Either of these methods requires that a variable coefficient matrix be inverted in the semi-implicit method. Once the principle of solving a variable coefficient problem is accepted, many of the uncomfortable compromises forced by the need to extract a constant coefficient matrix disappear. For instance, there is no need to use a basic state profile to derive the equations or the integration scheme. The need for such profiles has brought the ability to run global nonhydrostatic models into question, Golding (1992). The multigrid method is currently the favoured method for variable coefficient elliptic problems, being faster and more robust than conjugate gradient methods. This advantage appears to remain on massively parallel computers though it is diminished (Mawson, private communication). Much basic work has been done on the ability of different finite difference horizontal grids to represent the geostrophic adjustment process. Arakawa and Lamb (1977) show that the C grid represents this process and the resulting balanced state best unless the grid size is greater than the Rossby radius, about 3000km for modes of the full tropospheric depth and 1000km for modes with an equivalent depth of 1km. The unified model grid size is less than this for all production configurations. (Note that this conclusion does not apply to the ocean where the Rossby radius is smaller and the B grid is best for grid lengths over 100km).

In the vertical, the geostrophic adjustment process is improved if the horizontal velocities and temperatures are held at different levels in the vertical, Arakawa (1983). This allows the most compact possible stencil for representing the thermal wind equation. This grid was introduced by Charney and Phillips (1953) and was used in the Meteorological Office 10 level model. It has been found necessary to use it to allow accurate solutions to balanced models in a vertical cross section, Cullen (1989). This grid has been unfashionable recently because it is harder to satisfy an exact energy equation in the manner demonstrated by Arakawa and Suarez (1983). However, we have shown in this paper that the energy conservation requirement can be met by changes to the semi-implicit formulation. The advantages of the grid in geostrophic adjustment have been recently demonstrated by Leslie and Purser (1992). The use of such a vertical staggering has

advantages for data assimilation in that it is easy to calculate balanced height increments to match wind increments. A 20% error is typical when computing height increments to match given wind increments, and then recalculating the wind increments from the height increments (Andrews, private communication). However, it is less convenient for the boundary layer scheme. It is proposed that the model layer boundaries are at levels where horizontal wind components are held, with potential temperatures at layer midpoints. Thus potential temperatures map directly onto layer thicknesses. The surface layer for potential temperature is thus twice as thick as that for wind. Above this, the bulk Richardson number is calculated at layer boundaries using temperature differences between two layer midpoints, but an average vertical wind shear from two adjacent layers. Mixing coefficients are then derived for heat, moisture, and momentum at layer boundaries. The momentum mixing coefficients are then interpolated horizontally and vertically to where fluxes are being calculated. Similar techniques need to be used in the gravity wave drag scheme. Though these interpolations may prove a disadvantage, on the current vertical grid the smallest vertical scale in potential temperature is invisible to the dynamics because it gives a zero impact on the pressure. However, such a pattern has a major impact on the parametrization, as the fluxes between potential temperature layers depends on the lapse between each pair of layers. Thus a dangerous decoupling between physics and dynamics is possible.

The main recommendations are therefore:

i) Semi-implicit with multigrid solver for variable coefficient problem.
ii) C grid horizontally
iii) Charney-Phillips grid vertically.
iv) Height as vertical coordinate.
(v) Horizontal interpolation of pressure correction.

References

Arakawa, A. 'Vertical differencing of the primitive equations',

Proc. ECMWF Seminar on Numerical Methods for Weather Prediction, 1983, Vol.1, 207-224.

Arakawa, A. and Lamb, V.R. 1977 'Computational design of the basic dynamical processes of the UCLA general circulation model',

Methods in Comp. Phys., 17, Academic Press, 174-265.

Arakawa, A. and Suarez, M. 1983 'Vertical differencing of the primitive equations in sigma coordinates',

Mon. Weather Rev., 11, 34-45.

Charney, J.G. and Phillips, N.A. 1953 'Numerical integration of the quasi-geostrophic equations for barotropic and simple

baroclinic flows',J.Meteor., 10, 71-99.

Clark, T.L. 1977 'A small-scale dynamic model using a terrain following coordinate transformation'. J.Comp.Phys.,24,188-215.

Cullen, M.J.P. 1989 'Implicit Finite Difference Methods for modelling discontinuous atmospheric flows', J. Comp. Phys. 81, 319-348.

Cullen, M.J.P., Davies, T., Mawson, M.H., 1992 'Conservative finite difference schemes for a unified forecast/climate model', UM Documentation paper no. 10.

Dudhia, J. 1991 'A nonhydrostatic version of the Penn State/NCAR mesoscale model', NCAR preprint submitted to Mon. Weath. Rev.

Golding, B.W. 1992 'An efficient non-hydrostatic forecast model'. Meteor. Atmos. Phys. 50, 89-103.

James, J.A. 1992 MSc Thesis, University of Reading.

Laprise, R. 1992 'The Euler equations of motion with hydrostatic pressure as an independent variable'. Mon. Weath. Rev. 120, 197-207.

Leslie,L.M. and Purser,R.J. 1992 'A comparative study of the performance of various vertical discretization schemes'.Meteorol.Atmos.Phys. 50, 61-73.

White, A.A. and James, J.A. 1991 'Recommendations for the development of the dynamics of the mesoscale model'. Short Range Forecasting Res. Div. Tech. Note no. 61.

Mesoscale Effects of a dry intrusion within a vigorous cyclone

B.W.Golding

Meteorological Office,
London Road, Bracknell, Berks. RG12 2SZ

A modelling study has been carried out to complement the observational study conducted by Prof. K. A. Browning of a developing depression and cold front that crossed the UK on 12th November 1991 producing violent squalls and at least two tornadoes.

The model used was the updated version (described in Golding, 1992, Meteorol Atmos Phys 50,89-103) of the old UKMO mesoscale model. It was initialised by interpolation from a 6-hour assimilation, ending at 12UT, of the mesoscale version of the UKMO Unified Model running at 16.8km grid spacing. An important feature of this assimilation was the inclusion of the Valentia ascent which had been rejected in quality-control tests by the regional version of the Unified Model (grid length 50km).

The simulation was run at 15km resolution, on a 92x92 domain covering the British Isles, with 16 levels in the vertical at 10,110,310,610,1010m.... Various combinations of parametrizations were included to elucidate the processes involved, and full advantage of the model's graphical diagnostics package was taken in investigating the relationship between descending, dry, high potential vorticity air; and ascending, saturated, high potential vorticity air in the frontal zone.

Preliminary results suggest that the development of the frontal squall was associated with the intrusion of dry, high potential vorticity air into the pre-frontal warm conveyor belt in the 1-4 km height range. Work is continuing on the relationship between the model diagnostics and the observations, and it is also planned to use the model at much finer resolution to investigate details of the interaction.

OBSERVATION AND MODELLING OF THE AGGREGATION PROCESS IN A FRONTAL RAINBAND: THE 21st OF JUNE CASE STUDY.

Virginie MARECAL, Anthony J. ILLINGWORTH and Susan P. BALLARD

University of Reading - UK Met. Office,
Reading, United Kingdom

1. INTRODUCTION

Frontal precipitation is usually organised on the mesoscale into rainbands of different types (Hobbs, 1978). Warm frontal rainbands (WFRs) are about 50-100 km wide, oriented parallel to the warm front, located ahead or at the surface warm front and associated with aloft tropospheric vertical motions. In the past, several WFRs have been studied using radiosoundings, radar observations and aircraft mesurements (e.g. Browning and Harrold 1969, Locatelli and Hobbs 1987). It appears that above the warm frontal zone, a shallow layer of potentially unstable air is usually observed and tends to generate active convective cells (called generating cells). The small ice crystals initiated by the generating cells aloft grow by vapour deposition and mainly by aggregation while falling into the stratiform cloud layer below (Hobbs and Locatelli 1978, Herzegh and Hobbs 1980, Matejka et al. 1980). This mechanism leads to a noticible precipitation enhancement at ground level on the mesoscale. Aggregation is thus a dominant process in precipitation formation whithin WFRs. It has to be well evaluated in models in order to get a good precipitation forecast and it is generally poorly represented.

A warm frontal rainband passed over England on the morning of the 21 June 1990. It has been simultaneously sampled by the Chilbolton radar and the Met. Office C130 aircraft. These measurements clearly show that aggregation is very active in precipitation generation. In parallel, a non-hydrostatic mesoscale forecast model (Golding, 1992) is used to simulate this rainband. The microphysical scheme and in particular the aggregation representation has been modified according to the observation in order to better simulate the rainband.

2. OBSERVATIONS

2.1 General situation

On the 21 June 1990, an occluded frontal system passed over the British Isles. A WFR associated with this system has been followed from 0600 UTC by the UK Met. Office FRONTIERS operational radar network. It is about 100 km wide and located ahead and parallel to the warm front and to the occlusion (see Fig. 1). Two reflectivity cores (corresponding to a rainfall rate (RR) of more than 4 mmh^{-1}) are embedded in the rainband.

2.2 Chilbolton radar observations

During the rainband passage, the dual-polarisation Chilbolton radar performed mainly RHI scans (140 km range) at 235° North orientation every 5 minutes on average. The scans were made nearly perpendicular to the rainband (see Fig. 1) and unfortunately did not sample the two precipitation maxima within the rainband. In figure 2 is depicted the reflectivity RHI scan at 1123 UTC. The bright band which corresponds to the melting layer is well defined. This suggests that mainly ice precipitation is present above the 0°C level. The LDR (linear depolarisaton Ratio) and ZDR (differential reflectivity) fields provided by the dual polarisation signals exhibit the signature of the presence of aggregates above the 0°C level. Moreover, the steep gradient in reflectivity in the 500 m above the bright band suggests that aggregation process is active. The rain region located under the bright band in fig. 2 is not uniform with more intense precipitation zones of several

kilometres. This and the wavy pattern that appears aloft might be interpreted as trails of precipitation. This is similar to the reflectivity pattern that can be observed in the presence of generating cells (Browning and Harrold 1969, Herzegh and Hobbs 1980, Locatelli and Hobbs 1987). It is not possible to be fully sure since there are no radar kinematic fields.

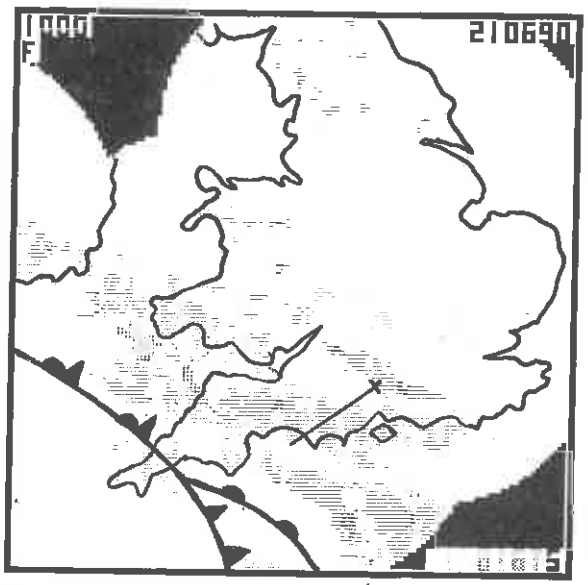

Figure 1: Rainfall rate in mmh^{-1} at ground level at 1000UTC from the Frontiers radar network. The surface fronts are displayed according to the surface observations. The cross shows the Chilbolton radar location and the heavy line corresponds to the trace of the RHI scans. The legend is at the bottom of the figure (< 1, > 1, > 4, > 8 and > 16 mmh^{-1}).

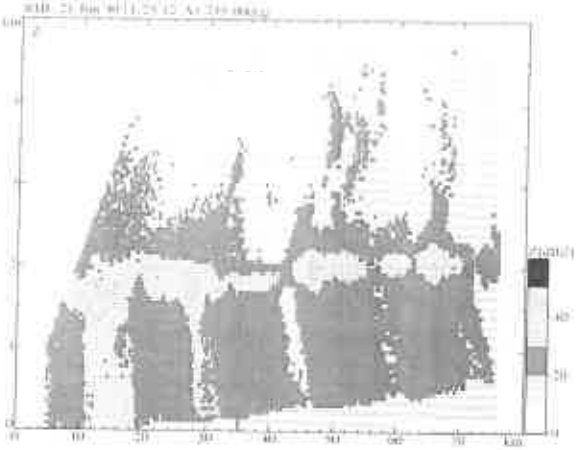

Figure 2: Chilbolton RHI scan at 235° North at 1123 UTC.

2.3 Aircraft microphysical measurements

Aircraft measurements were performed nearby and within the Chilbolton RHI scans plane between 0950 UTC and 1211 UTC by the Met. Office C130 aircraft. The aircraft legs were done between the -2°C and +2°C levels (2.1 to 1.3 km height above ground level). This sampled layer is interesting since the maximum precipitation growth seems to occur just above the 0°C level (see fig. 2). The following microphysical probes were mounted on board the aircraft: a FSSP, a 2DC and a 2DP Knollenberg image probes.

The qualitative analysis of the 2DC and the 2DP images shows that in the 0°C to -2°C layer, large particles recorded are mainly rimed aggregates. Riming is consistent with the presence of cloud water recorded by the FSSP: 0.15 gm^{-3} (mean) and 0.35 (max).

The size-distribution $N_i(D)$ of the sampled ice particles follows an exponential form:

$$N_i(D)=N_{0i}\exp(-\lambda_i D) \qquad (1)$$

For each 10s sample, the N_{0i} and λ_i coefficients have been determined by a least square fit.

These values are compared to Passarelli (1978)'s work on aggregation. He constructed an analytical model of aggregation and vapour deposition growth of an exponential size-distribution of ice particles. An important result of this study is that in the case of steady stratiform precipitation, N_{0i} and λ_i will tend to an equilibrium relationship given by $N_{0i}=C\,\lambda_i^3$, where C depends on the updraft velocity, the temperature lapse rate and the snowfall type.

The (N_{0i}, λ_i) couples determined from the ice particles 2DP images have been plotted and fitted using a least-square fit method (fig. 3). The relationship obtained is:

$$N_{0i}=C\,\lambda_i^x \qquad (2)$$

with $C=1.15\ 10^{-3}\ m^{x-4}$, x=2.9 and a good correlation coefficient of 0.95. Relationship (2) is very close to Passarelli (1978)'s model. This suggests that, in the sampled layer, aggregation is one of the major ice growth processes. Riming is probably acting as well (as discussed before). This process does not affect the size-distribution in the the absence of large variations in the collection efficiency with particles size.

3. MODEL DESCRIPTION

3.1 General description

The model used in this study is the latest version of the UK Met. Office mesoscale forecast model. Its characteristics are described in detail in Golding (1992, 1993). It is non-hydrostatic, fully compressible with a semi-implicit time integration and a semi-Lagrangian advection. The model includes a bulk microphysical scheme with a representation of ice processes which has been improved according to the observations.

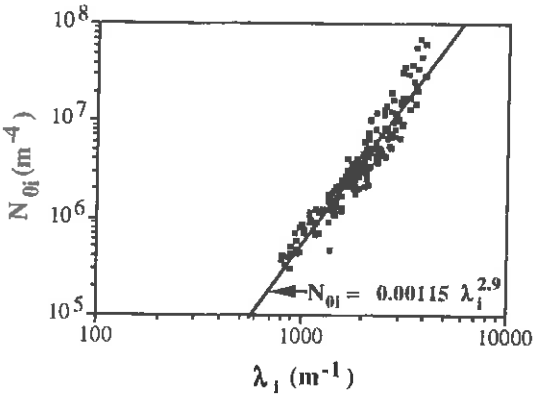

Figure 3: N_{0i} plotted as a fuction of λ_i. The solid line corresponds to the least square fit.

3.2 The improved microphysical scheme

The analysis of the observations (section 2) suggested that riming and aggregation are the dominant processes in the ice precipitation generation within the layer 0°C to -2°C (maximum precipitation growth layer). Riming is a process which is fairly well evaluated in models. On the other hand, aggregation is usually ill-represented. Thus, the problem is : what is the best approach to represent aggregation in the model ?

In models including ice phase processes via a bulk-parameterisation, the ice content (or mixing ratio) is usually divided at least into two categories: cloud ice with a negligible fallspeed and ice precipitation (one or several types) (Cotton et al. 1982, Lin et al. 1983, Rutlegde and Hobbs 1983). This approach allows to take into account the fact that precipitation type and thus precipitation characteristics usually vary with the size of particles due to different initiation and growth processes. Ice precipitation is usually assumed to follow an exponential form with a constant N_{0i}. Ice aggregation is represented by two mechanisms: the autoconversion of cloud ice into precipitation and the accretion of cloud ice by ice precipitation. The autoconversion parameterisation is very ill-controled.

We have chosen to use a different approach. Here, the basic idea is to represent all ice crystals by only one variable: q_i, the mixing ratio of ice. Since q_i includes both small and large particles, q_i is not modified by the aggregation process which is an ice particle-ice particle interaction. Thus, aggregation does not have to be represented in the model by an ill-controled parameterisation. Our approach is physically correct only :

- if one can assume that the simulated rainband contains one very dominant type of ice particles and
- if the model is able to well represent the characteristics of all ice crystals. In other terms, it means that the size-distribution, the mass-dimension and the fallspeed-dimension relationships chosen in the model have to be valid for all particles sizes.

The analysis of the 2D probes aircraft data supports this approach. The sampled particles are, for a very large majority, rimed aggregates as shown by the 2DC and 2DP probes images. The assumption of one type of particles is thus realistic. Moreover, all the particles follow a continuous exponential shape distribution with a dependence between N_{0i} and λ_i given by (2). This represents the aggregation effect on the ice size-distribution. Consequently, the microhpysical scheme of the model has been modified and now includes the observed relationship (2). The problem of using the aircraft data is the representativeness. The aircraft probes sampled a small area with respect to the horizontal dimension of the rainband and a the shallow layer (-2° to +2° C). On the other hand, this layer is where ice particles growth is maximum according to the Chilbolton radar observations and thus it is the most important in terms of microphysics.

The mass-dimension relationship for ice was determined from the aircraft

measurements. The fallspeed-dimension relationship is from Locatelli and Hobbs (1974).

4. MODEL RESULTS

The model is run with a 15 km horizontal grid-spacing and 16 vertical levels above orography (10, 110, 310, 610, ... 12010 m). The domain is 1320 by 1350 km^2 and covers the British Isles. The model is initialized at 0000UTC (operational mesoscale model forecast). The boundary conditions (every 3 hours) are from fine-mesh model forecast (75 km resolution).

4.1. Reference run results

The reference run has the characteristics described above. In figure 4 is represented the RR at ground level given by the model at 1000 UTC. Note that the domain displayed is smaller than the actual calculation domain and is centered around the rainband location. Compared with the observations (fig. 1), the 1 mmh-1 contour is well simulated by the model and maximum values are close to the observations (14 mmh^{-1} simulated and 16 mmh^{-1} observed). On the other hand, the 4 mmh-1 contour is more extended in the model runs. On average, precipitation at ground level is overestimated. Another difference is the location of the intense precipitation zones within the rainband which is not well predicted by the model. This is probably related to the surface front location which is shifted by about 100 km with respect to the observations (see fig. 4). This seems to be due to an error in the large scale forcing imposed by the boundary conditions.

Figures 5ab represent a vertical cross section perpendicular to the rainband (see fig. 4) of θ_e (equivalent potential temperature) and of 'water' content (rain + ice). The warm frontal zone is well marked (see fig. 5a). A convectively unstable zone is located above the rainband. No radiosounding have been launched in the rainband and thus it is not possible to validate this result. Nevertheless, this feature has been observed in the past (e.g. Browning and Harrold 1969, Locatelli and Hobbs 1987). In fig. 5b, the

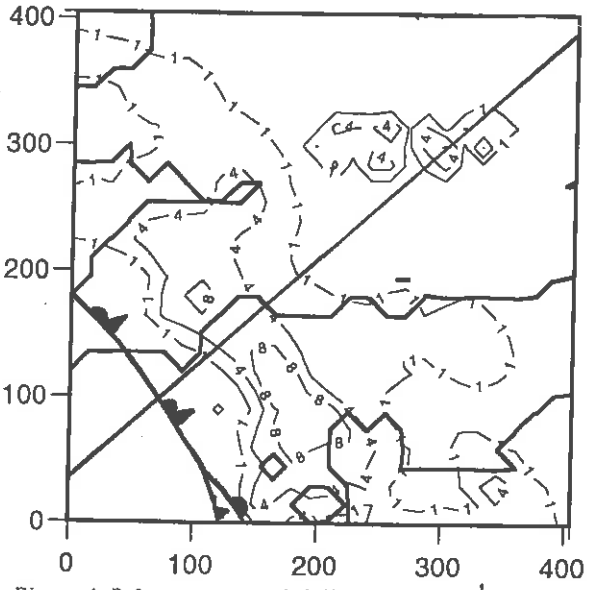

Figure 4: Reference run: rainfall rate in mmh^{-1} at ground level at 1000 UTC simulated by the model. The surface fronts are located according to the model. The solid line gives the location of the vertical cross section displayed in fig 6 and 7. The domain is 405 by 405 km^2.

maximum ice precipitation content is predicted just above the 0°C level as observed by the Chilbolton radar. It is located below the potentially unstable layer. This suggests the presence of generating cells. These cells are of a few kilometres horizontal extension and cannot be resolved by the model which has a 15 km resolution. However, the model simulates an ice precipitation initiation in the unstable layer and an important growth of ice particles while falling. The maximum ice content simulated is similar to that calculated by the aircraft probes (about 0.35 gm^{-3} over a 15 km horizontal distance).

4.2. Sensitivity tests

4.2.1. Cloud ice/precipitation ice scheme

The model was also run with a microphysical scheme including the classic representation of ice and aggregation:

- two variables for ice are solved in the model: cloud ice and ice precipitation,
- ice precipitation size-distribution follows an exponential form with a constant N_{0i}. The N_{0i} value chosen corresponds to the mean N_{0i} recorded by the aircraft 2DP probe,
- autoconversion of ice (aggregation) is represented by the classic

parameterisationgiven by Rutledge and Hobbs (1983).

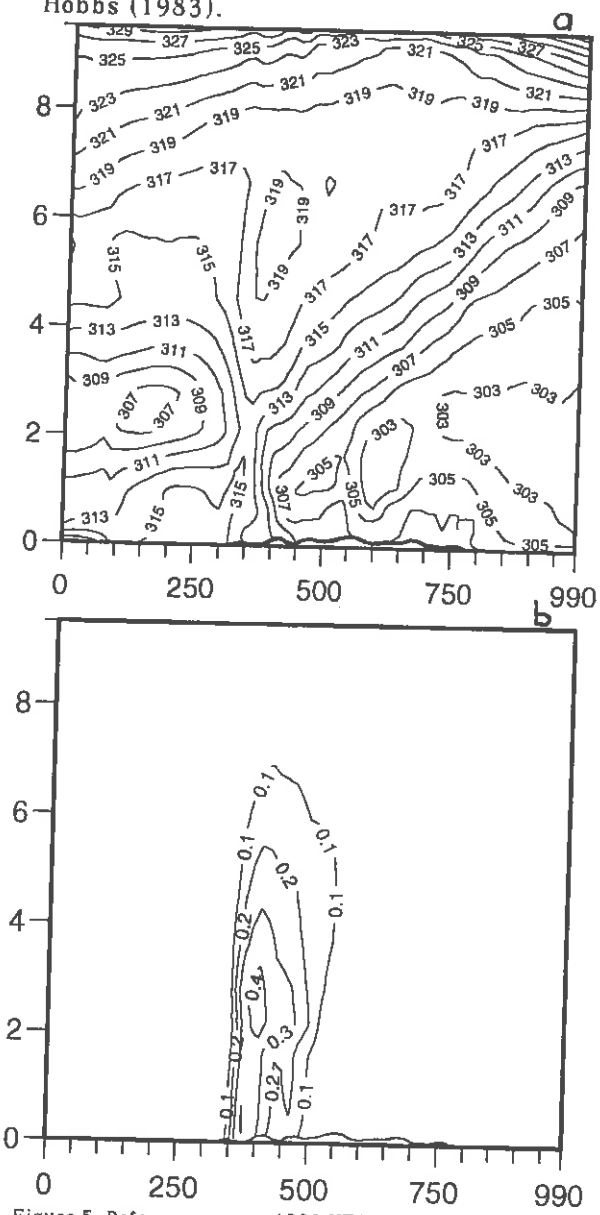

Figure 5: Reference run at 1000 UTC: vertical cross-section perpendicular to the rainband (see fig 4) of (a) θ_e (in K) and (b) precipitation content (in gm^{-3}). The horizontal scale is 990 km.

No important differences with the reference run of the ground level RR can be noted. The reference run gives on average slightly less precipitation. The vertical cross-section of precipitation content is very different in the ice region (fig. 6). The maximum qi for this 'classic' scheme is twice as much as in the reference run and from the aircraft probes. Thus, the reference run gives more realistic results (in terms of ice simulation) even if it overestimates the precipitation content at ground level. Note also that the reference scheme solves at least one equation less and thus is cheaper in terms of computer time.

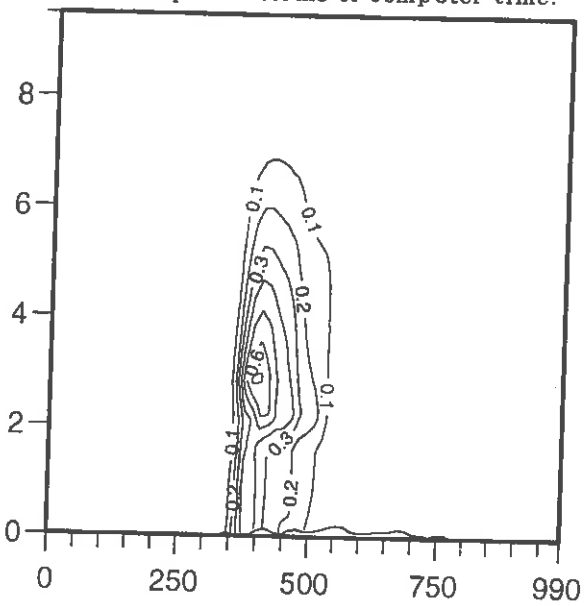

Figure 6: Run with a classic parameterisation (see text): Rainfall rate at ground level (in mmh^{-1}) at 1000UTC. The hosizontal scale is 990 km.

4.2.2 Run with 5km horizontal resolution

The model was run with 5 km horizontal grid-spacing on a limited area domain located around Chilbolton location (405x405 km^2). The model is initialised at 0000 UTC as for the reference run. Boundary conditions are from the reference run.

The ground level RR (fig. 7a) found is much more realistic than the 15 km run. Within the 1 mm h^{-1} contour, a 50 km wide precipitation core is simulated. It is very similar to the main core observed by the Frontiers radars (South of Wales). The maximum values predicted by the model are 14 mmh^{-1} which is very close to the observed values. The core location is about 100 km too far South East with respect to the observations. This location difference is probably due (as for the 15 km run) to a large scale forcing error (via the boundary conditions). In fig. 7b is displayed a vertical cross section parallel to the Chilbolton RHI but shifted by 100 km South East (to take into account the simulation shift with respect to reality). The rain content at ground level is very similar to that recorded

by a disdrometer located nearby Chilbolton. In the ice region, the ice content aloft is consistent with the Chilbolton observations. On the other hand, the maximum ice content is lower (0.2 gm^{-3}) than that recorded by the aircraft.

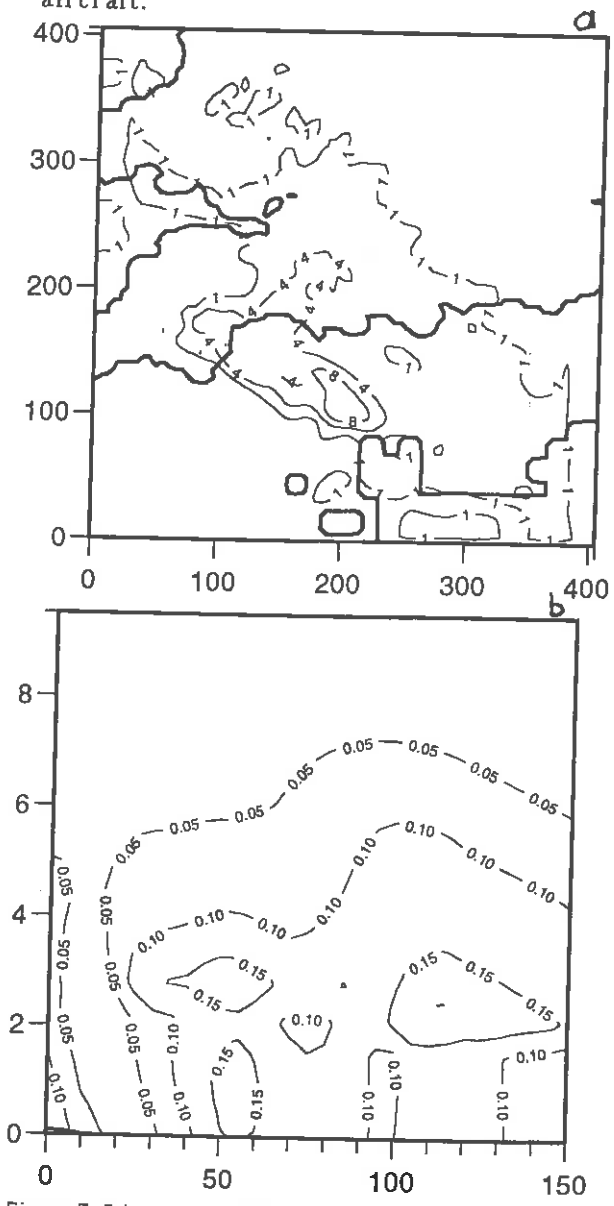

Figure 7: 5 km run at 1000UTC: (a) rainfall rate at ground level in mmh^{-1} and (b) vertical cross section perpendicular to the rainband of water content in gm^{-3} (see text): 150 km horizontal scale.

5 CONCLUSION

The radar and aircraft measurements have shown that ice precipitation within the WFR is mainly created by riming and aggregation just above the 0°C level. They fit well Passarelli's (1978) theory of aggregation and are consistent with previous observational studies.

The microphysical scheme of a mesoscale forecast model has been modified according to the observations results. The major results are:

- precipitation seems to be initiated aloft in a potentially unstable layer,
- the reference run overestimates the overall precipitation at ground level,
- the reference run new scheme gives better results in the ice region than a classic microphysical scheme,
- the 5 km horizontal resolution run gives far better results than the 15 km run.

This work shows that the precipitation simulation, in particular in WFRs, can be improved by introducing measured parameters in the microphysical scheme. The combined use of observations and a model is a good approach to understand the microphysics.

REFERENCES

Browning, K.A., and T.W. Harrold, 1969: Air motion and precipitation growth at a wave depression. *Quart. J. Roy. Meteor. Soc.*, 95, 288-309.

Cotton, W.R., M.A. Stephens, T. Nehrkorn and G.J. Tripoli, 1982 : The Colorado State University three-dimensional cloud/mesoscale model. Part II: An ice phase parameterization. *J. Rech. Atmos.*, 16, 295 - 320.

Golding, B.W., 1992: An efficient non-hydrostatic forecast model. *Meteorol. Atmos. Phys.*, 50, 89-103.

Golding, B.W., 1993: A numerical investigation of tropical island thunderstorms. *Mon. Wea. Rev.*, 121, 1417-1433.

Herzegh, P.H. and P.V. Hobbs, 1980: The mesoscale and micropscale structure and organization of clouds and precipitation in Midlatitude cyclones. II: Warm-frontal clouds. *J. Atmos. Sci.*, 37, 597-611.

Hobbs, P.V., and J.D. Locatelli, 1978: Rainbands, precipitation cores and generating cells in a cyclonic storm. *J. Atmos. Sci.*, 35, 230,241.

Locatelli, J.D. et P.V. Hobbs, 1974: Fallspeeds and masses of solid precipitation particles. *J. Geophys. Res.*, 79, 2185 -2197.

Locatelli, J.D. and P.V. Hobbs, 1987: The mesoscale and microscale structure and organization of clouds and precipitation in midlatitude cyclones.

Matejka, T.J., R.A. Houze Jr and P.V. Hobbs, 1980: Microphysics and dynamics of clouds associated with mesoscale rainbands in extratropical cyclones. *Quart. J. Roy. Meteor. Soc.*, 106, 29-56.

Passarelli, R.E., 1978: An approximate analytical model of the vapor deposition and aggregation growth of snowflakes. *J. Atmos. Sci.*, 35, 118-124.

Rutledge, S.A., and P.V. Hobbs, 1983: The mesoscale and microscale structure and organization of clouds and precipitation in midlatitude cyclones. Part VII: A model for the "seeder-feeder" process in warm-frontal rainbands. *J. Atmos. Sci.*, 40, 1185-1206.

PARAMETERIZATION OF POLLUTANT TRANSPORT IN CONVECTIVE CLOUDS.

Neil Gimson, JCMM, University of Reading.

Introduction.

It has long been recognised that cumulus clouds play an important role in the transport, chemical transformations, and removal of pollutants. Recent observational programmes (Ching and Alkezweeny, 1986; Tremblay, 1987), using aircraft measurements bear this out, demonstrating the effects of strong updraughts in raising low-level contaminants and thus "cleaning" the boundary layer. Also evaporatively cooled downdraughts bring material from above the boundary layer down to lower levels. Precipitation reaching the surface may produce localised deposition of pollutants which are attracted to water droplets, such as soluble gases or hygroscopic aerosols. Recent three-dimensional cloud-resolving cloud chemistry models also show these, and other, effects (Tremblay and Leighton, 1986; Niewiadomski, 1989).

In a mesoscale model, cumulus clouds are sub-gridscale, and their influence must therefore be parameterized. This article describes the derivation of a scheme in which a simple one-dimensional time-dependent model is used to represent transport by up- and down-draughts contained in a single grid-square. Parameterizations of the convection itself have existed for at least twenty years, but consideration of their effects on transient tracers is more recent (see Gidel (1983), for a tracer scheme based on the Ogura and Cho (1973) cumulus parameterization). It is postulated here that transport by sub-gridscale convection in mesoscale models, where the model timestep is much shorter than typical convective transport times, must be treated differently to that in larger scale models. Only vertical transport is considered here (diffusion, chemistry, and removal are disregarded), and results are compared with those from a cloud-resolving "large eddy" model with the same initial sounding.

Conservation of a passive tracer.

The mesoscale grid square is divided into the area occupied by the cloud updraughts and downdraughts and the environment around the clouds. The conservation of a tracer moving in vertical columns of height-dependent

cross-sectional area may be expressed as

$$\frac{\partial(\rho_1 A_1 \chi_1)}{\partial t} + \frac{\partial(M_1 \chi_1)}{\partial z} = E_1 \chi_3 - D_1 \chi_1 \qquad 1(a)$$

$$\frac{\partial(\rho_2 A_2 \chi_2)}{\partial t} + \frac{\partial(M_2 \chi_2)}{\partial z} = E_2 \chi_3 - D_2 \chi_2 \qquad 1(b)$$

$$\frac{\partial(\rho_3 A_3 \chi_3)}{\partial t} + \frac{\partial(M_3 \chi_3)}{\partial z} = - E_1 \chi_3 + D_1 \chi_1 - E_2 \chi_3 + D_2 \chi_2 \qquad 1(c)$$

where ρ_j is the air density, A_j area, $M_j = \rho_j A_j w_j$ air mass flux, w_j vertical velocity, and j = 1, 2 or 3 for up-, down-draught and environment respectively. χ_j is the tracer mixing ratio (note $\chi_j \equiv 1$ for air mass continuity). The right hand sides of (1) represent exchange of air between columns due to entrainment (resp. detrainment) at a rate E_j (resp. D_j).

The steady-cloud scheme.

Equations 1(a-c) may be combined to produce an equation for the grid-area mean tracer $\bar{\chi}$. This is traditionally done in large-scale models for thermodynamic variables (recently Tiedtke, 1989; Gregory and Rowntree, 1990), and may be easily extended to include pollutants - this was first done by Gidel (1983). This leads to

$$\frac{\partial(\bar{\rho}\,\bar{\chi})}{\partial t} + \frac{\partial(\bar{\rho}\,\overline{w}\,\bar{\chi})}{\partial z} = - \frac{1}{A} \frac{\partial(M_1(\chi_1 - \bar{\chi}) + M_2(\chi_2 - \bar{\chi}))}{\partial z}, \qquad (2)$$

where overbars denote grid-area means and $A = A_1 + A_2 + A_3$, the grid area itself. The solution of (2) requires M_1, χ_1, M_2 and χ_2. These are calculated in 1(a) and 1(b), neglecting the time derivatives. This will be called the "steady-cloud" scheme, as the in-cloud quantities are obtained in this approximate way. Equations 1(a) and 1(b) become

$$\frac{\partial M_j}{\partial z} = E_j - D_j \qquad j = 1,2. \qquad 3(a),(b)$$

and

$$\frac{\partial(M_j \chi_j)}{\partial z} = E_j \bar{\chi} - D_j \chi_j \qquad j = 1,2. \qquad 4(a),(b).$$

With prescribed entrainment and detrainment rates, (3) gives the mass fluxes and (4) gives the pollutant fluxes to be used in (2), which is solved without the need for individual areas, densities, and vertical velocities.

The unsteady-cloud scheme.

However, solving 4(a) instead of 1(a) means that contaminant can be raised through the depth of the column in one time-step. This may be realistic in global or climate models, but not in mesoscale models where the timestep is of the order of one minute. The solution of (2), (3) and (4) will be compared with a scheme in which the in-cloud time-derivatives (those in 1(a) and 1(b)) are retained. In fact, (1) is solved without further manipulation or approximation. This will be called the "unsteady-cloud" scheme.

Results.

The large-eddy model (LEM) was run with 500m horizontal resolution, having 40×40 grid intervals and 32 levels in the vertical. It was initialised with a convectively unstable sounding taken from mesoscale model output, with the cloud base diagnosed at 1265m and cloud top at 5085. Fluxes of heat and moisture from the sea surface were included, to initiate convection in the LEM. A horizontally uniform contaminant distribution was introduced after 100 minutes, centred 2km above the surface. Resulting tracer concentration ($\overline{\rho\chi}$) profiles are shown in Fig. 1. Material spreads in the vertical, up to cloud top levels (between 6 and 7 km) and down near to the surface. At later times, the "bulge" appearing at a height of 200m becomes a local maximum (not shown).

The LEM output data suggests $M_1 = 3.2\times10^7$ kgs^{-1} between cloud base and top levels. Setting $M_2=M_3\equiv0$, 3(a) is solved for E_1 at cloud base and D_1 at cloud top (elsewhere they are zero). Then 4(a) is solved for χ_1 and (2) for $\bar{\chi}$. Profiles of $\bar{\chi}$ are shown in Fig. 2, for an initial plume centred at the cloud base level. Material appears at the cloud top level, but none is ever seen at the intermediate levels. This can be compared with Fig. 3, where $A_1 = 22.5\text{km}^2$, $A_2 = 0$, and $A_3 = 202.5\text{km}^2$, and 1(a) and 1(c), the unsteady-cloud equations, are solved. In this case the plume rises gradually through the cloud. Significantly, at 30 minutes there is no pollutant at height 5km, while in the steady-cloud scheme, there is a large fraction of the plume there. It is this discrepancy that leads to the conclusion that the steady-cloud approximation to (1) is not appropriate in a mesoscale model parameterization.

Setting $M_2 = -4.9\times10^6$ kgs^{-1} at cloud mid-level, decreasing to -9.8×10^6 kgs^{-1} at cloud base, increasing to zero at the surface, $A_2 = A_1$, $A_3 = 180$ km^2, a subsidence velocity $w_3 = -15$ cms^{-1} at in-cloud levels,

$E_1 = D_1 = M_1/1500$ at these levels, and deducing E_2 and D_2 from 3(b) such that both are positive. These parameters are suggested by output from the LEM, and adjusted such that the total contaminant mass raised (resp. lowered) above (resp. below) the initial plume top (resp. base) is the same for the unsteady-cloud scheme as the cloud-resolving LEM results. The resulting profiles are plotted in Fig. 4 for an initial plume centred at 2km, and are comparable with those in Fig. 1.

Summary.

In a parameterization of sub-gridscale tracer transport in a mesoscale model, it is necessary to integrate the in-cloud concentrations in time. Quantities χ_1 and χ_2 must therefore be carried by the model in addition to the grid-box mean, $\overline{\chi}$. Some adjustment of mass fluxes and entrainment rates may be required as the scheme is further developed, but this basic conclusion should still be valid.

It is our intention to convert the one-dimensional unsteady-cloud scheme described above into a true parameterization, that is, to relate in-cloud quantities to the "mesoscale" mean quantities, under some closure assumption(s). Then the scheme will be implemented in the UKMO non-hydrostatic mesoscale model, to study the effects of convection on pollutant dispersion in a three dimensional model.

References.

Ching J.K.S. and A.J. Alkezweeny, 1986: Tracer study of vertical exchange by cumulus clouds. *J. Clim. Appl. Met.*, **25**, 1702-1711.

Gidel L.T., 1983: Cumulus cloud transport of transient tracers. *J. Geophys. Res.*, **88**, 6587-6599.

Gregory D. and P.R. Rowntree, 1990: A mass flux convection scheme with representation of cloud ensemble characteristics and stability dependent closure. *Mon. Wea. Rev.*, **118**, 1483-1506.

Niewiadomski M., 1989: Sulphur dioxide and sulphate in a three-dimensional field of convective clouds: numerical simulations. *Atmos. Env.*, **23**, 477-487.

Ogura Y. and H.-R. Cho, 1973: Diagnostic determination of cumulus cloud populations from observed large-scale variables. *J. Atm. Sci.*, **30**, 1276-1286.

Tiedtke M., 1989: A comprehensive mass flux scheme for cumulus parameterization in large-scale models. *Mon. Wea. Rev.*, **117**, 1779-1800.

Tremblay A., 1987: Cumulus cloud transport, scavenging and chemistry: observations and simulations. *Atmos. Env.*, **21**, 2345-2364.

Tremblay A. and H. Leighton, 1986: A three-dimensional cloud chemistry model. *J. Clim. Appl. Met.*, **25**, 652-671.

1. LEM results.

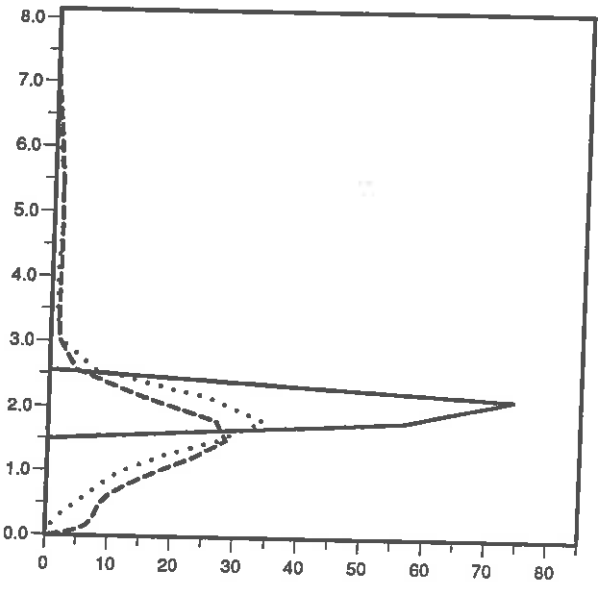

2. Steady-cloud scheme.

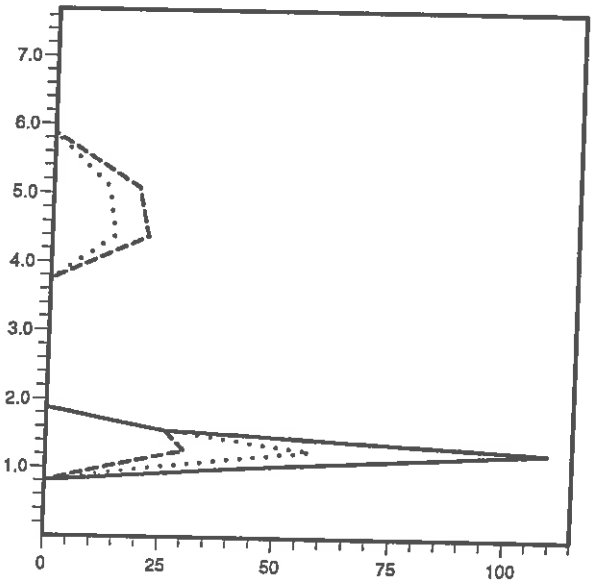

3. Unsteady-cloud scheme.

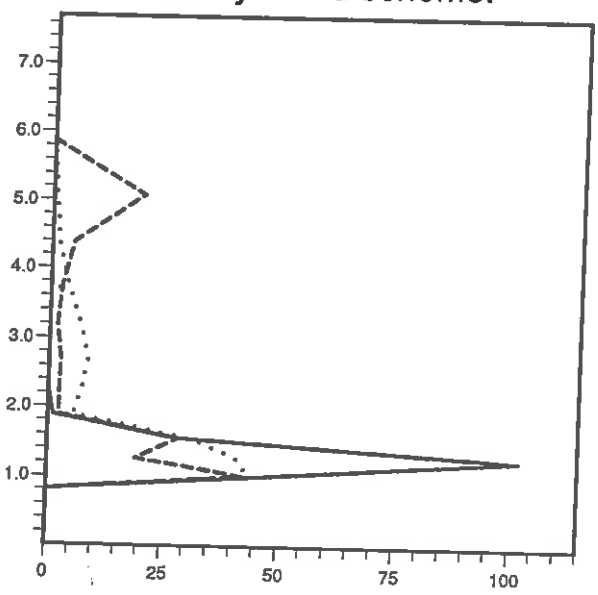

4. Downdraught and subsidence.

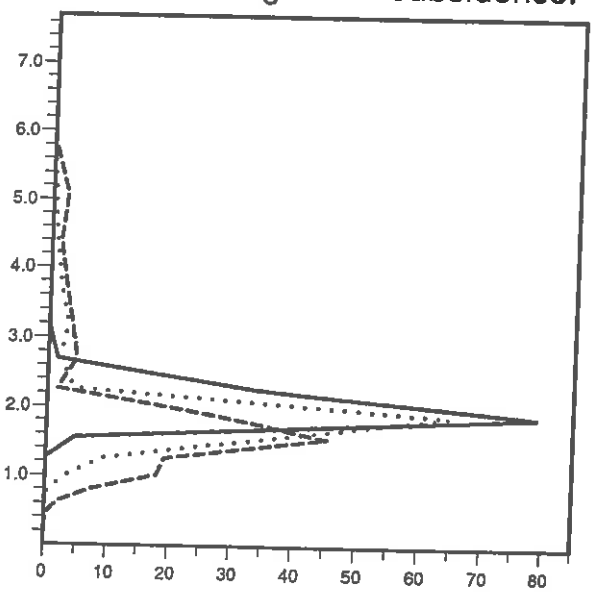

Tracer profiles: Concentration along horizontal axis; vertical axis is height in km. Profiles are for the initial time (solid), and after 30 (dotted) and 60 (dashed) minut es.

MODELLING THERMALLY-DRIVEN FLOWS OVER VALLEY-SIDE SLOPES

B. W. Atkinson
Queen Mary and Westfield College,
University of London

1. Introduction

This project is concerned with the modelling of thermally-generated flows over slopes and valleys at the meso-gamma scale. The more particular aims have been to assess the effects of stability and orography on up-slope flows within a valley. The model used is the UK Meteorological Office meso-scale model. It is mounted on both the Queen Mary and Westfield College DRS 6000 and the University of London Convex computers and all runs mentioned in this report were done on the latter machine.

2. The experiments

The model has been used to conduct experiments in idealised case studies of flows over slopes in valleys. The valley is specified by a simple quadratic function (Eq 1):

$$E = \frac{by^2}{a^2 + y^2} \qquad 1)$$

where a is the half-valley width, b is the maximum orographic height and y is the north-south horizontal distance. The particular configuration used in the experiments described here was an open-ended valley with no tilting of the floor and oriented along a north-south line. The domain was 21x21x16 grid points.

Extensive testing of the effects of variations in horizontal grid lengths, horizontal diffusion coefficients, time steps, the inclusion or exclusion of the convection sub-routines on model results led to the choice of horizontal grid lengths of 4km, a time step of 40s and horizontal diffusion coefficients of K_m=15000 and K_h=7500. Such a configuration allowed maximum run length of 12 hrs. Grid lengths of 3 km allowed runs of just under 9 hrs before model breakdown, whereas lengths of 1km allowed runs of only 2.7 hrs. All these tests were done in a valley with maximum slopes of about 5 deg.

The stabilities used in the experiments were described by linear lapse rates throughout the depth of the domain. Values ranged from isentropic to +1.0 deg C/100m Slope magnitude was primarily determined by varying b in Eq 1. The effect of the shape of valley cross-section was assessed by changing the value of a in Eq 1. In all the experiments the relative humidity was set to 5%. This value is sufficiently low as to prevent cloud formation (an undesirable complication at this stage), yet high enough to prevent numerical complications.

3. Results

The experiments were conducted for upslope flows. The initial conditions were set for mid-day on 21 June at the latitude of southern England. The stabilities were set as described above and the initial velocities were set to zero. The valley-side slopes were changed by setting b equal to 500, 1000, 1500, 2000 and 4000m in successive

experiments where a was held at 16km. The valley cross-section shape was changed by setting a equal to 4, 8, 12, 16, 20, 24 and 28km in successive experiments where b was held at 1500m. The runs were started at mid-day and lasted for three simulated hours, the results thus giving conditions for mid afternoon.

The effects of initial stability and slope angle on cross-section averages of horizontal $\overline{|u|}$ and vertical $\overline{w}$ components of velocity are summarised in Fig 1. Due to the virtually symmetric distribution of the horizontal component within the valley its absolute value is used in the averaging. It is clear from both parts of this figure that two distinct regimes, dependent upon stability, emerge in both the $\overline{|u|}$ and $\overline{w}$ fields. The threshold stability between these regimes is 0.03 - 0.04 deg C/100m. At stabilities marginally greater than 0.04 deg C/100m the lowest values of $\overline{|u|}$ and the highest value of $\overline{w}$ are found. At yet higher stabilities the velocity components are far less sensitive to stability variations than in the unstable regime. Nevertheless the u component increases with stability to maxima at 0.1-0.15 deg C/100m before gently reducing in magnitude with further increases in stability. The w component shows a consistent decline with increasing stability. The effects of slope magnitude are also shown in Fig 1. At stabilities lower than the threshold value the horizontal component is quite sensitive to b, decreasing as b increases from 500 to 1500 and then increasing again (Fig 1a). The case where b = 4000m was probably beyond the limit of the model's capability to handle steep slopes, thus explaining its lack of consistency with the other cases. Fig 1b shows the same kind of result for vertical velocity, revealing the robustness of the two stability-governed regimes. At stabilities higher than the threshold value, clear relationships emerge between the velocity components and slope angle. Vertical velocity increases virtually linearly as b increases. The relationship for the horizontal velocity is more complex (Fig 2). It increases virtually linearly with b up to value b = 2500m (mean slope angle of about 3-5deg), and then decreases to b = 3500m (mean slope angle of 5deg).This relationship may well be related to the cross-section size of the valley and its associated topographic amplification factor. At values b $\leq$ 2500m, the valley is open enough to allow the circulation to increase as the thermal forcing on the steeper slopes increases; at values b > 2500m, the decreased cross-section area constrains the development of the horizontal velocity, but has little effect on the vertical velocity.

The effects of valley half-width (a) on the flow field were investigated for the case where b = 1500m. A small value of a gives a V-shaped valley, with a relatively small cross-section area: a large value of a gives a U-shaped valley with a larger cross-section area. Large values of a also reduce the mean slope angle between valley-side and bottom but the difference between the slope values of a = 8km and 28km is only one-fifteenth of the difference due to the range of slope values ensuing from the changes in b investigated above. Consequently the results of this analysis give a fair assessment of the effects of variation in valley-width on valley slope flows. Fig 3a again reveals two distinct regimes of $\overline{|u|}$ dependent upon stability, with the same threshold as previously identified. In initial stabilities greater than about 0.04 deg C/100m, $\overline{|u|}$ varies with both stability and orography. Between stability values of 0.05 deg C/100m and 0.5 deg C/100m, the horizontal velocity is inversely related to a, the narrow valley shape giving the largest values of $\overline{|u|}$. In this regime, the maximum values of $\overline{|u|}$ are also directly related to stability in addition to their relationship with orography. In the case with a = 8km, the maximum $\overline{|u|}$ occurs with a stability of 0.1 deg C/100m, whereas with a = 28km, the maximum $\overline{|u|}$ occurs with a stability of 0.5 deg C/100m. At a stability of 0.5 deg C/100m, a reversal takes place: at values of stability greater than this threshold,

horizontal velocities become directly related to a, but magnitudes generally are lower than in the stability range 0.1-0.5 deg C/100m.

Vertical velocity is also dependent on the two major stability regimes (Fig 3b) and at stabilities greater than about 0.04 deg C/100m shows maxima at 0.05 deg C/100m and decreasing values to 0.4 deg C/100m. Thereafter the values remain quasi-constant at low magnitude, with little sensitivity to variations in a. However, in the stability range 0.05 to 0.4 deg C/100m vertical velocities show an inverse relationship with a, in similar fashion to that shown by $|\overline{u}|$. These results show that, for given values of valley depth and side-slope angle, the magnitudes of flow speed over valley slopes vary inversely with valley width, but that the relationship for the horizontal component is sensitive to stability. This relationship between the airflow and valley width should be considered to lie within a stronger relationship between airflow and slope angle. Fig 2 shows that flow speed increases with b, but that for each value of b, an increase in a reduces the speed of the flow.

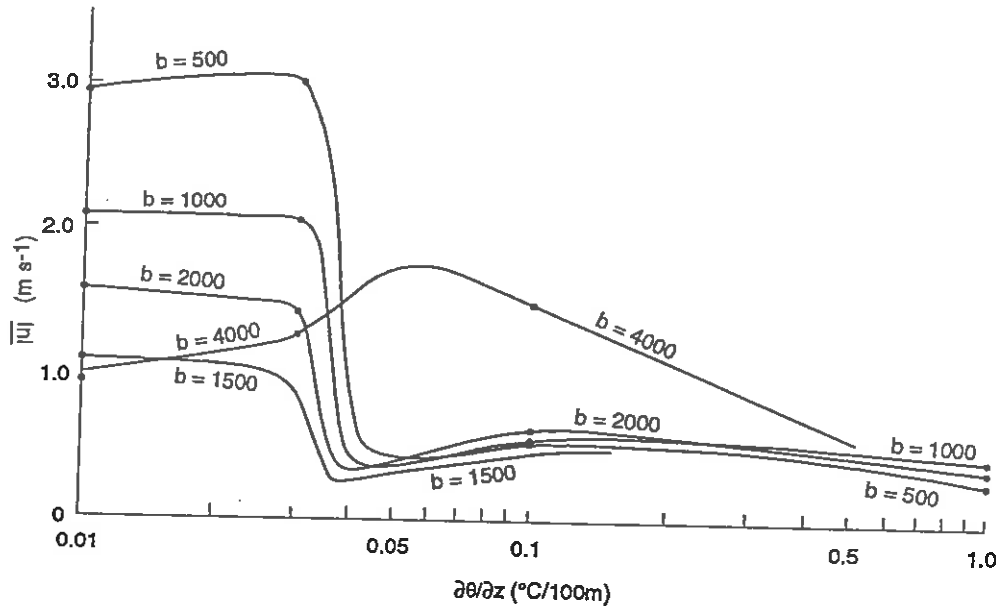

1(a) Cross-section mean of across-valley (horizontal) component of velocity ($\overline{|u|}$) (ms^{-1}) against initial stability (deg C/100m) a = 16km, b = 500, 1000, 1500, 2000, 4000m

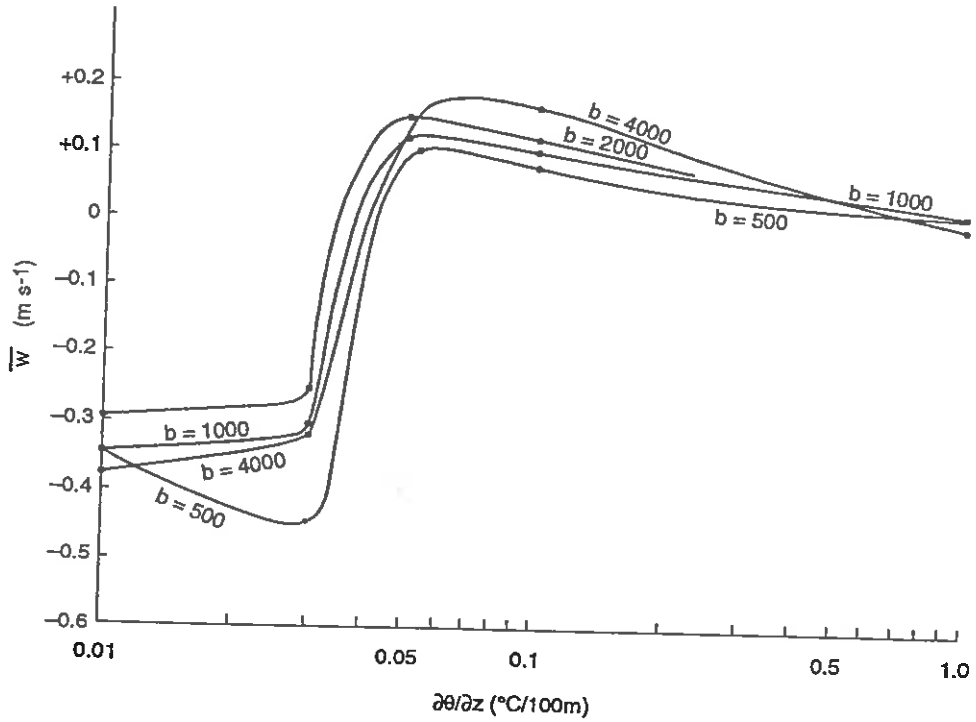

1(b) Cross-section mean of vertical velocity component ($\overline{w}$) (ms^{-1}) against initial stability (deg C/100m) a = 16km, b = 500, 1000, 1500, 2000, 4000m

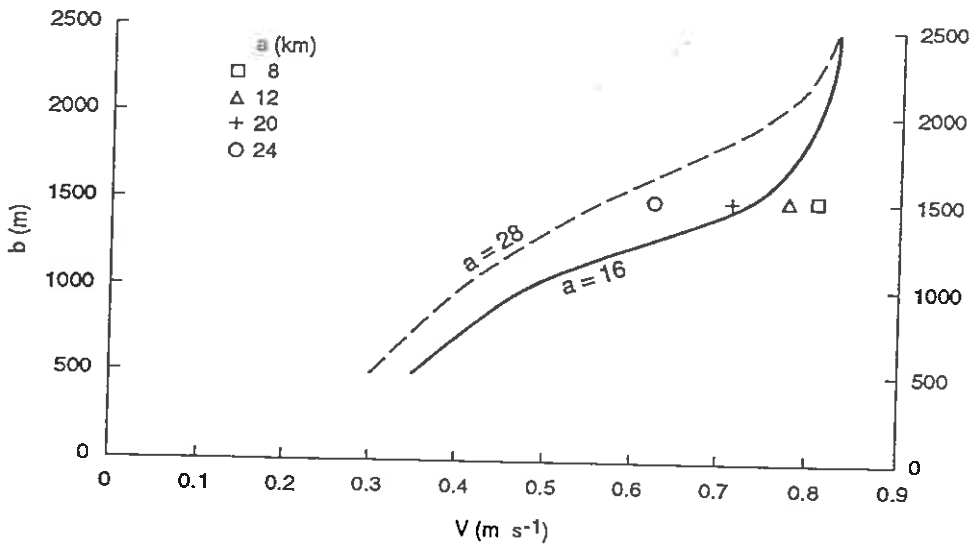

2 Cross-section mean of velocity (**V**) (ms^{-1}) against b for initial stability of 0.4 deg C/100m and a = 16km and 28km. Other symbols along b = 1500m give values of (**V**) for a range of values of a

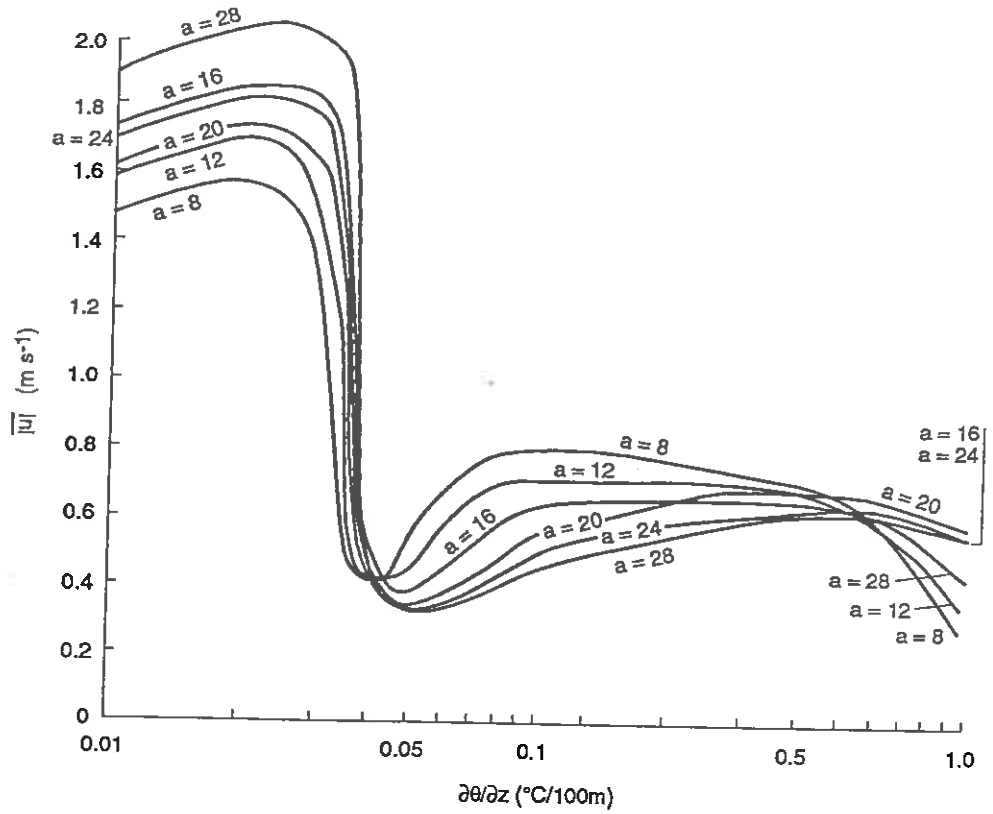

3 (a) Cross-section mean of across-valley (horizontal) component of velocity ($\overline{|u|}$) (ms^{-1}) against initial stability (deg C/100m) $b = 1500$m, $a = 8, 12, 16, 20, 28$km

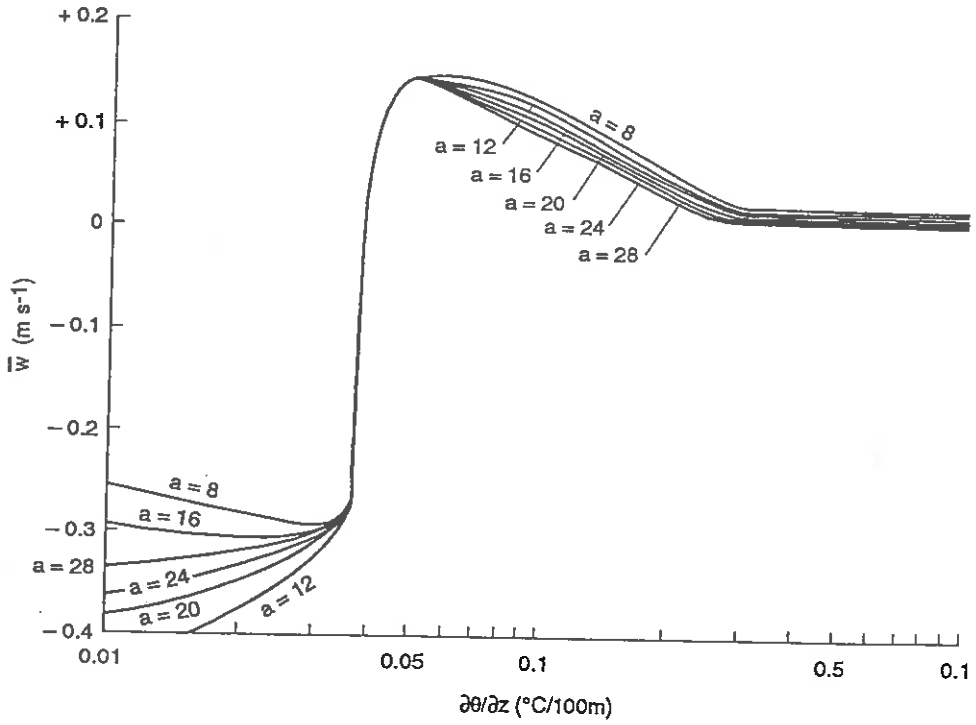

3(b) Cross-section mean of vertical velocity component ($\overline{w}$) (ms^{-1}) against initial stability (deg C/100m) $b = 1500$m, $a = 8, 12, 16, 20, 24, 28$km

HIGH RESOLUTION NUMERICAL SIMULATIONS OF FLOW OVER THE PYRENEES: PYREX IOP 3

Adrian S. Broad
U.K. Meteorological Office
Bracknell, England

Summary : The 'old' operational U.K. Meteorological Office Mesoscale model is used to simulate a lee wave event from the PYREX mountain experiment. The resulting quasi-steady state integration is used to diagnose surface pressure drag and vertical momentum fluxes, and to analyse two counter-rotating lee vortices. Wave stresses from the model are compared against grid box values taken over the Pyrenees in the climate version of the U.K. Met Office's unified model.

1. INTRODUCTION

An idealized version of the U.K. Meteorological Office's 'old' operational non-hydrostatic Mesoscale model with 32 vertical levels (rising to 17.11 Km) is used to simulate lee vortices and lee wave motion over the Pyrenean mountain range. Data from the PYREX mountain experiment of 1990 is used to initialise the model and verify the resulting integration, the aim of the present work being to compute the pressure drag and vertical momentum flux profiles for validating and improving sub-grid gravity wave drag parametrization schemes within NWP models. The PYREX program was a major field study of the dynamical influence of a major mountain range on the atmospheric circulation focussing particularly on diagnosing the momentum budget. Results from the model focus on one particular Intensive Observing Period (IOP3: 14 and 15/10/90) during which a Southerly wind impinged on the Pyrenees generating large amplitude lee waves.

The numerical model is configured to run on a regular 2km grid with 90×120 points (in the 'x' and 'y' directions respectively) and with a vertical separation of 600m above 2.11km upto a height of 17.11km. The horizontal domain covers the central portion of the Pyrenees and uses a smoothed orographic height field (Fig. 1) derived from a 500m resolution dataset. Wave reflection at the upper boundary is prevented by a stratospheric damping layer where horizontal diffusion coefficients increase linearly from a background tropospheric value of $500m^2s^{-1}$ at (and below) 10.51km, to $25000m^2s^{-1}$ at the model top. In conjunction, Newtonian damping is applied above 10.51km relaxing temperature and velocity components to their upstream values with a time constant which decreases exponentially with height. In the experiments all surface energy fluxes are switched off and the relative humidity set equal to 1% to ensure a dry integration. The model is initialised with a single upstream radiosonde ascent taken from Zaragoza, Spain at 00Z 15/10/90. Vertical smoothing is applied to the wind and temperature fields and horizontal velocities are taken to be constant. Pressure and temperature variations are subsequently derived assuming linearity consistent with the geostrophic and thermal wind relations respectively. Figs. 2 (a), (b) and (c) show the unsmoothed wind speed, direction and temperature respectively taken from the ascent. The flow is SSW'ly above 1km below which the air is backed due to low level blocking by the Pyrenees (Fig. 2(b)).

2. RESULTS

The model is integrated for four hours after which time the orographically generated gravity waves have settled down to a quasi-steady state. The T+4 hr vertical velocity field is depicted at a height of 7km (Fig. 3) and as a vertical cross-section (Fig. 4) along

the line indicated in Fig. 3. A pattern of 'leaky' lee waves results with both hydrostatic and non-hydrostatic, trapped responses present. Peak vertical velocity amplitudes (upto $7ms^{-1}$) are in good agreement with observations, although the wavelength is too long ($\approx$ 20km as compared to 12km inferred from aircraft data). This is due primarily to certain limitations of the numerical integration procedure for which fixed upstream lateral boundary conditions are used. Transience in the upstream flow is therefore not directly modelled but maybe included by initializing the model with a different upstream radiosonde ascent. Such an integration, using 06Z 15/10/90 data from Zaragoza, gives better wavelength agreement ($\approx$ 15km).

Diagnosed areally averaged momentum flux profiles are compared directly with wave stresses resulting from the sub-grid scale gravity wave drag parametrization scheme in the climate version of the U.K. Met Office's unified model (Fig. 5). They appear to be in good agreement for this one case giving us some confidence in the parametrization scheme. This is provided of course that the stresses from the model are reasonable when compared with reality as inferred from PYREX measurements. Surface pressure drag calculations give us some confidence in this statement, the model being $\approx 3.3Nm^{-2}$ as opposed to an observed drag of $\approx 4.5Nm^{-2}$.

Detailed analysis of the model integration also shows two small scale counter-rotating vortices confined to the lower half of the boundary layer in the lee of the mountains (Fig. 6). These are dynamical effects resulting from the non-linearity of the flow at large non-dimensional mountain height numbers (Nh/U $>$ 1, N = Bouyancy frequency, h = mountain height, U = upstream velocity) caused by the height of the Pyrenees.

3. CONCLUSION

In order to refine gravity wave drag parametrization schemes used in NWP models there is a need for verification of these schemes against high resolution numerical model simulations and observational campaigns. PYREX offers one such observational database as a benchmark with which to compare areally averaged momentum budget calculations from experiments performed with high resolution models, and hence coarser scale models. The case study presented here shows the systematic workings, results and usefulness of this approach. The particular problem of the flow response and drag characteristics for large non-dimensional mountain height numbers is one which the PYREX dataset is able to address.

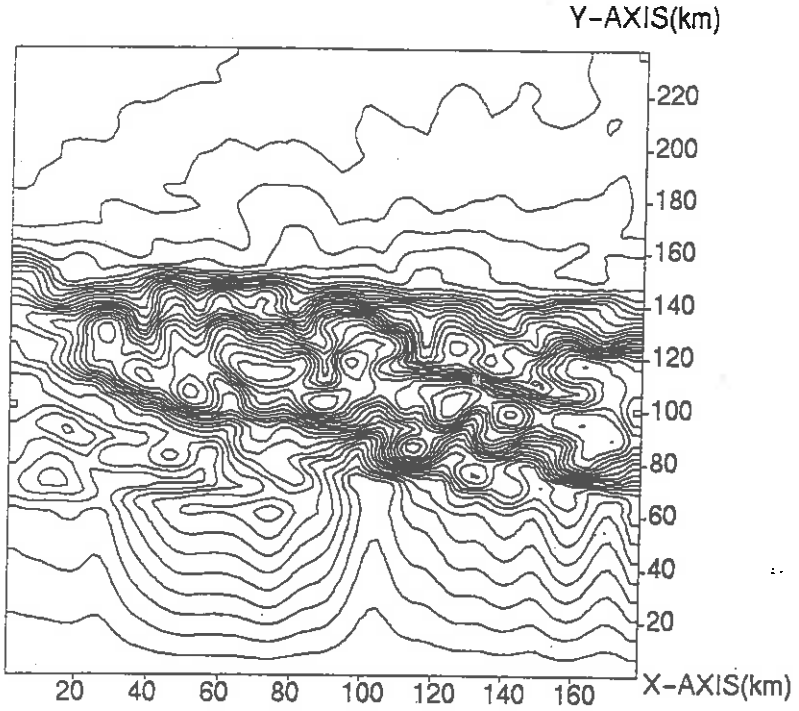

Fig. 1 Model terrain height map, contour interval $100m$.

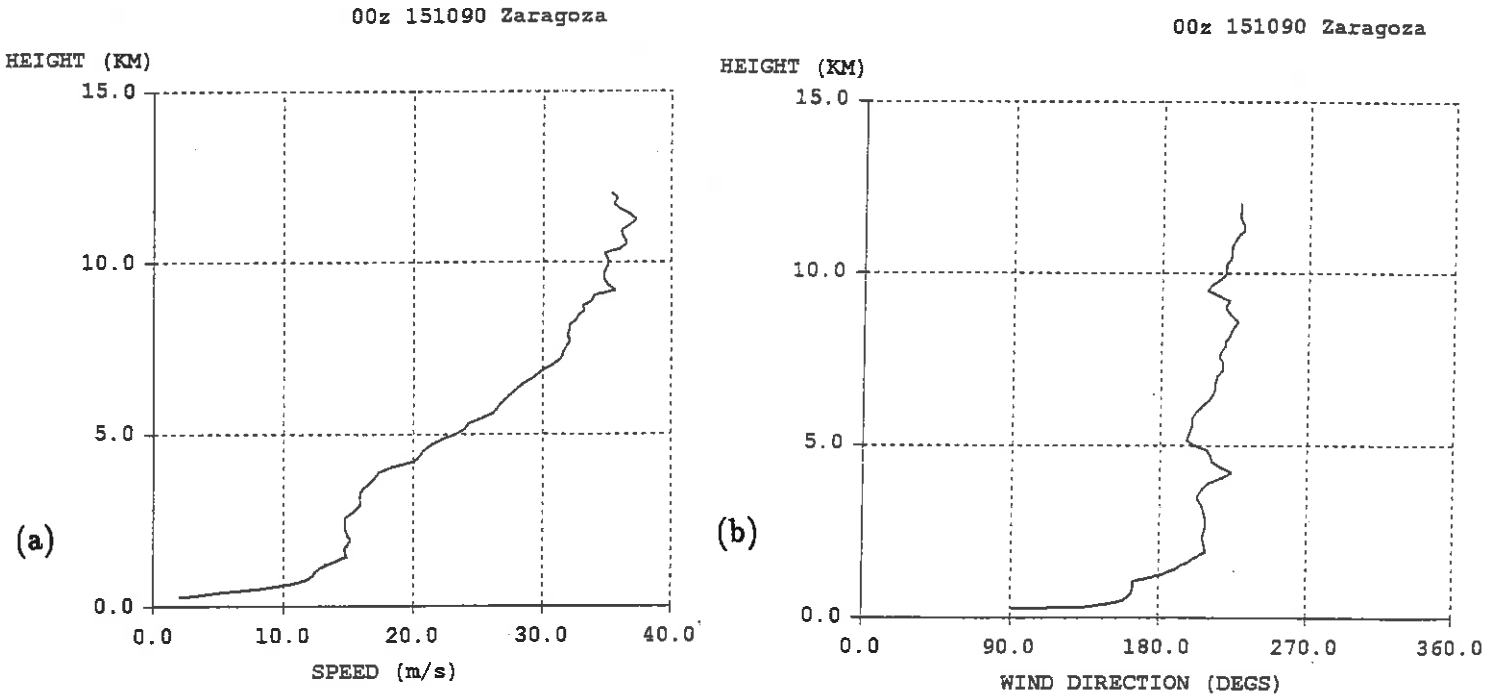

Fig. 2 Vertical profiles of (a) wind speed, (b) wind direction and (c) temperature obtained from the upstream radiosonde ascent.

Fig. 2(c)

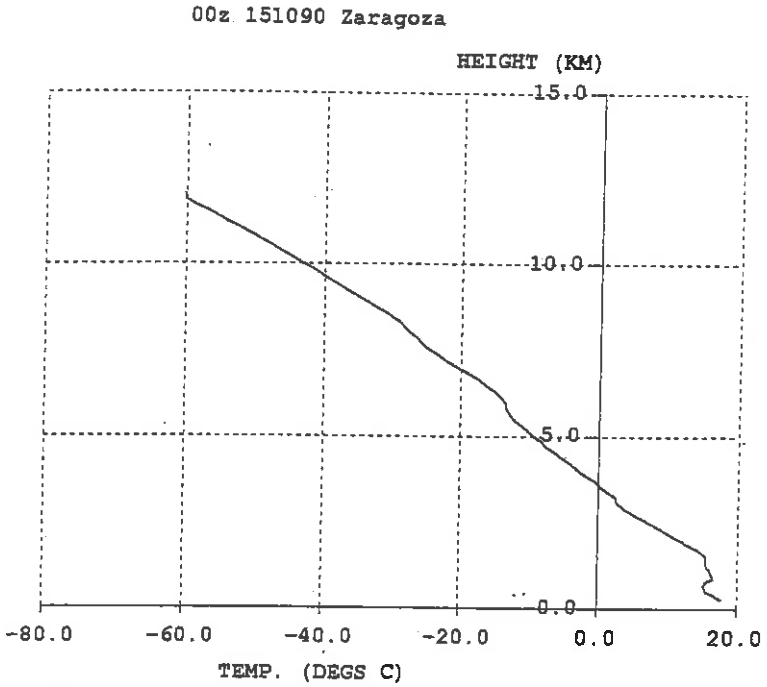

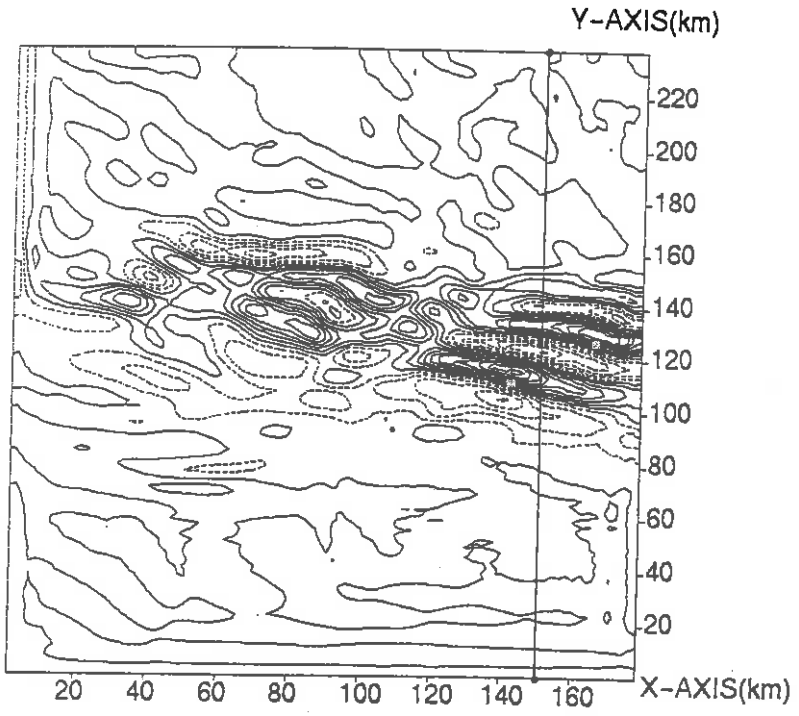

Fig. 3 Model vertical velocity field at $z = 7Km$ after four hours of integration. The line indicates the position of the vertical cross-section in Fig. 4. Contour interval: $1ms^{-1}$.

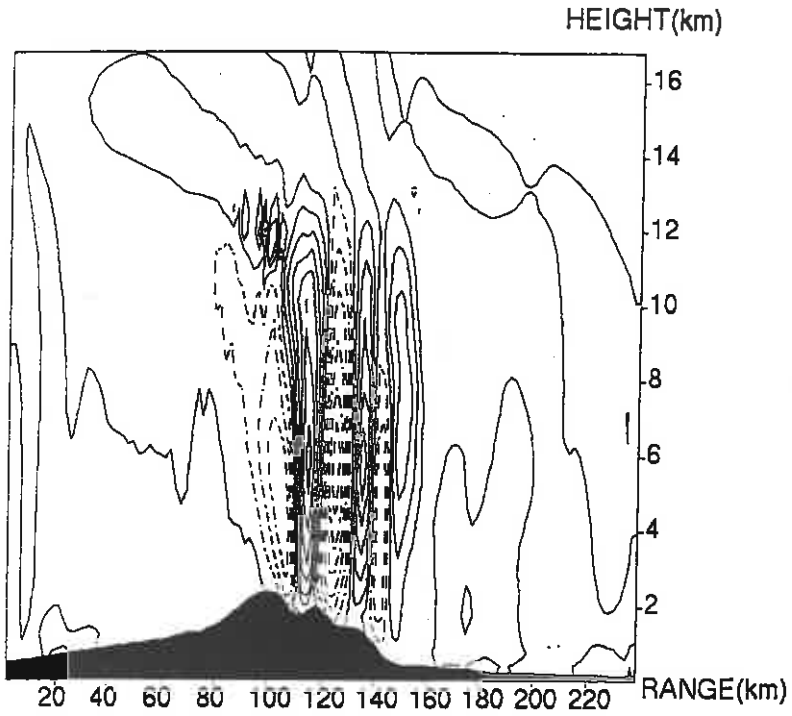

Fig. 4 Vertical cross-section of vertical velocity along the line indicated in Fig. 3. Contour interval: $1ms^{-1}$.

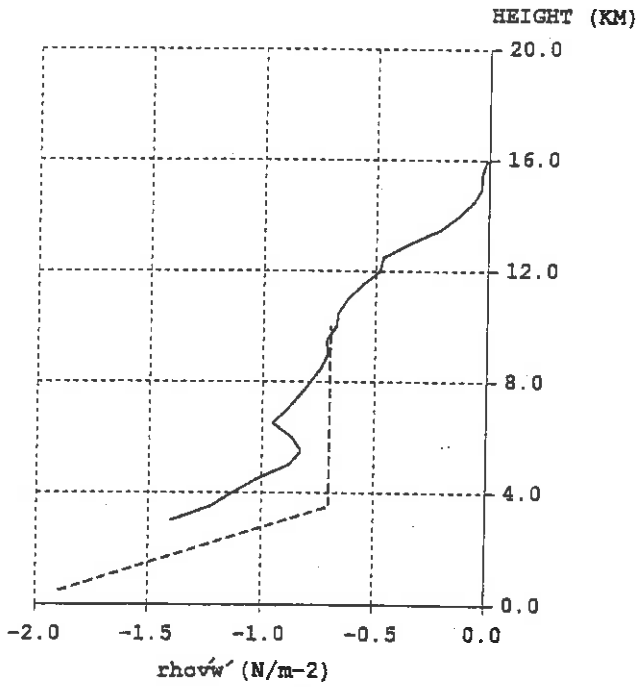

Fig. 5 Momentum flux profiles from the mesoscale model (solid line) and the climate version of the unified model (dashed line).

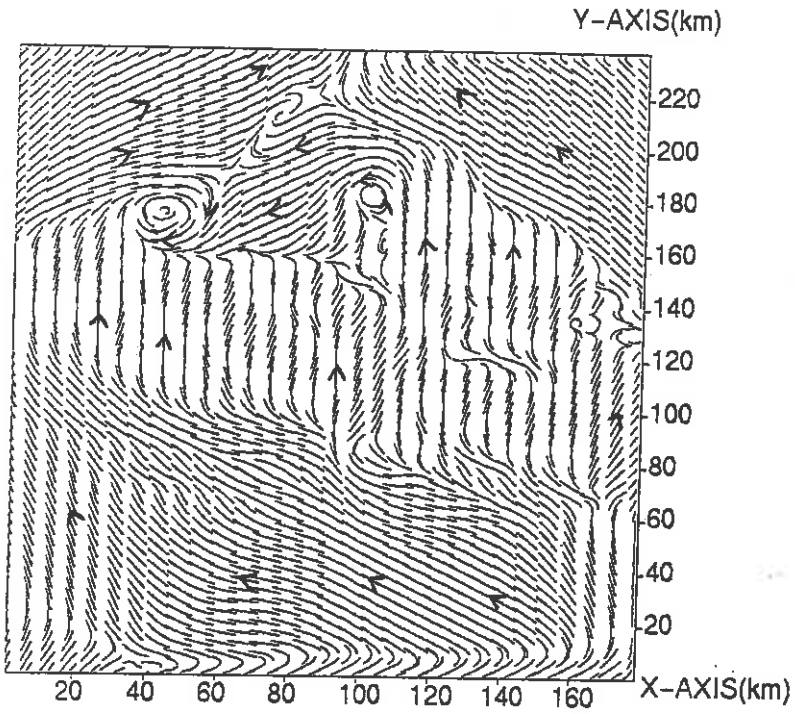

Fig. 6 Streamline plot of the 'horizontal' flow field (u and v velocities) at model level 2, 110m above the model surface.

Modelling Deep Convection

Roy Kershaw, Hugh Swann, Imtiaz Dharssi and Kozo Nakamura

Cloud Processes Group, JCMM

Introduction

In this article we describe progress made in the last year in developing and using a convective cloud model. The rationale for using the Met Office Large Eddy Simulation Model for modelling deep convection is discussed in Derbyshire and Kershaw (1993), and previous newsletter articles document the development of the model for this purpose: Shutts (1991) and Swann (1993). The aim of our project is to use the model to improve the parametrization of the effects of convection in larger scale models.

Recent work has shown that radiative effects can significantly modulate the behaviour of convective systems. Dudhia (1989) used a two dimensional simulation of convection over the south China sea to show that the large scale longwave cooling considerably enhanced convection by continuously destabilising the troposphere and thus countering the warming due to the convection. Tao et al (1992) simulated a tropical squall line and found that longwave cooling increased total rainfall by 31%. Hence we need to consider radiative effects in our model.

Model Development

During the year we have included parametrizations of ice processes and the effects of long wave radiation.

The microphysics scheme previously included only warm-rain processes. Water was represented by two mass-mixing ratio variables, rain and total non-precipitating water, cloud-water being a diagnosed quantity. A fuller representation of the role of water in cumulus clouds is achieved with the inclusion of three further water variables, ice cloud, snow and graupel. The conversion rates between categories are based on the bulk-water parametrization of Lin, Farley and Orville (1983). The assumption is made that the spectrum of sizes of each water particle type is inverse exponential and varies so that the mean diameter will increase as the amount of that water type increases. The phase changes and the rates of accretion of one particle to another can be expressed as functions

of diameter, so integrating over the size spectra gives total conversion rates and the mass-mean fall velocities. For a detailed description of the scheme see Swann (1994).

A further model variable was introduced to predict the number concentration of ice crystals. The processes that initiate ice crystals are many and varied and are very dependent on the specific conditions. Once a pristine ice crystal is formed it quickly grows by deposition or by accreting liquid water so the modelling of both number concentration and mass mixing ratio is desirable. The three initiation processes represented in the model are deposition onto natural ice nucleii, ice multiplication by splintering during the riming growth of graupel (the Hallett-Mossop effect) and contact nucleation of water droplets by natural aerosols. The latter two processes would be very difficult to model accurately without a predictive equation for the ice number concentration.

The longwave parametrization scheme implemented within the cloud model is based on the scheme used by the Unified model as described by Ingrams (1993) and Slingo and Wilderspin (1986). This makes use of the 'two stream' approximation whereby within each column only an upward and a downward flux are considered. This is only strictly valid for a plane-parallel atmosphere. For gaseous absorption, variations in the vertical are much larger than variation in the horizontal thus the 'two stream' approximation will give good results. However clouds can show significant horizontal variation and it is not clear how valid the 'two stream' approximation remains in this case. Unfortunately radiative schemes which include the horizontally finite extent of clouds are computationally very expensive and it remains impossible to include such a scheme within a cloud model.

The longwave radiative scheme includes absorption by water vapour, carbon dioxide, ozone, cloud water and cloud ice and is based on the commonly used broad-band transmissivity method. This method only includes the effect of absorption and emission and ignores scattering. Edwards (1992) has developed a new radiation scheme for the unified model which includes scattering in the longwave. However, it is generally believed that scattering is not important for longwave radiation. For gaseous absorption a lookup table is used to obtain transmissivities from absorber pathlength. This pathlength is scaled to include the effects of collision and doppler broadening of the absorption lines. For cloud water the transmissivity is calculated from an equation derived by Stephens (1984) using results from Mie Theory. Within the unified model cloud ice is treated in a similar way to cloud water. The absorption properties of ice are assumed to depend only on the ice water content and the difference in the absorption properties of ice and water is accounted for by a scaling constant. However, both experiment and theory show that this is incorrect and that the effective radius of the ice particles as well as the ice water content is important. Ignoring this leads to an over-estimation of absorption by cloud ice. The scheme within the cloud model has been modified to improve the treatment of cloud ice using a parametrization developed by Sun and Shine (1993). Also the effect of precipitation is now included (Dharssi 1994).

We have extended the diagnostic code to calculate the various components of the heat, moisture and momentum budgets, and verified that all three budgets balance. The facility to simulate the forcing effect of large scale ascent on convection has also been added.

Applications

Although the aim of our work is to model convective ensembles to formulate parametrizations for GCMs, the best way of validating the model is to carry out simulations of well-observed single-cell convection, so that model output can be directly compared to aircraft and radar measurements. The case studies chosen are the 22^{nd} June 1990 near the Chilbolton radar site, observed by both radar and the MRF C-130 aircraft, and the convective cloud studied during the 1981 Co-operative Convective Precipitation Experiment (CCOPE) in Montana, USA. The Chilbolton case had relatively warm cloud top of -15°C and produced a large amount of low density graupel. The CCOPE case had far more rapid growth with an updraught of 15m/s; hail stones were observed with diameters up to 7mm, and the cloud top was at 10.5km, where an anvil formed (figure 1).

Some of the parameters required by the microphysics scheme can be deduced from measurements made by the C-130's 2D probes, such as the intercept parameters that describe the size spectra of each particle type, and the particle density can be inferred from a combination of the radar and aircraft data.

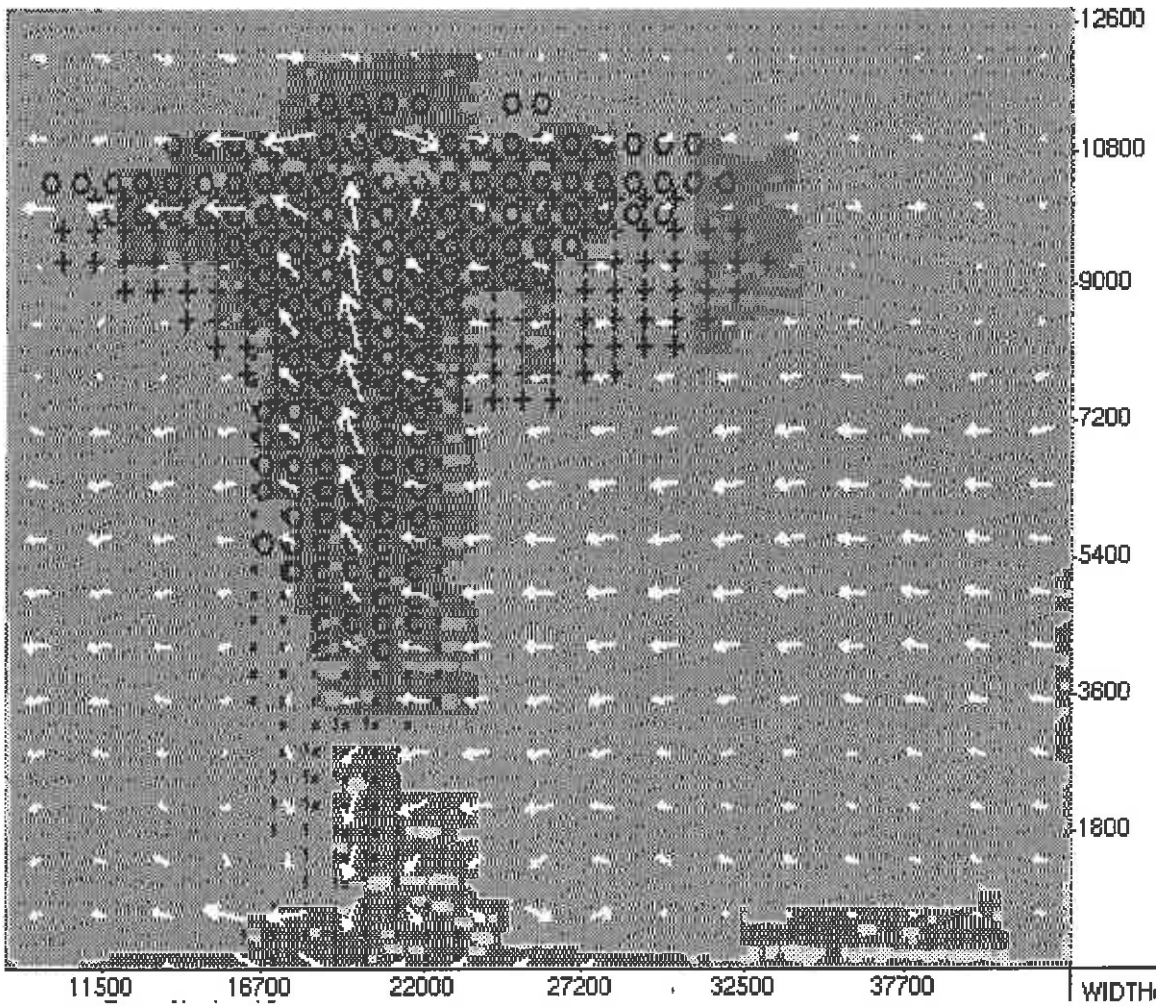

Figure 1: Vertical slice taken from the simulation of the CCOPE case study. Liquid cloud, rain, snow, graupel and ice cloud are represented by 'c's, commas, plus signs, fullstops and 'o's. The longest wind arrow represents a velocity of 15 m/s.

Many aspects of the parametrization can only be validated by comparing the evolution of the simulated cell to that observed. The model is initiated with the observed horizontal wind, temperature and humidity profiles but with zero vertical velocity. The convection is triggered by a moist warm bubble of air, large enough to cause a rising plume to reach the condensation level. With these simplified conditions, no orography and uniform surface fluxes, we can not hope to model exactly the evolution of a convective cell. The model should, however, predict key aspects of the development, such as the onset and extent of glaciation, the type and amount of precipitation, as well as the life time and size of the cloud.

We have made some modifications to the scheme in the light of these comparisons. The conversion rate of snow to graupel has been reformulated to include the effect of riming of liquid cloud, and the representation of the initiatiation and growth of ice crystals has been much improved. More extensive observations are required to validate the various assumptions in the microphysics scheme, such as the shape of the ice crystals, the size distributions of the hydrometeors, and their densities.

To validate the longwave radiation scheme within the cloud model we have made comparisons with observations obtained by MRF with the C-130. Figure 2 shows a comparison with the net longwave flux (upward minus downward) observed through a sheet of stratocumulus during a flight in the south Atlantic. The cloud model was run in single column mode with 51 vertical levels and initialized with observations from the C-130 and a nearby radiosonde ascent. The observed and calculated net fluxes are in good agreement except at cloud top. However the net flux increases rapidly near cloud top and even small errors in the height assignment of the measurements will result in large differences between the measured and calculated net fluxes. Thus the difference is likely to be due to either too high a height assignment of the measured fluxes or the cloud top height set too low within the model. It is interesting to note that by reducing the height assignment of the measured fluxes by 100 meters the agreement between the measured and calculated fluxes becomes almost exact.

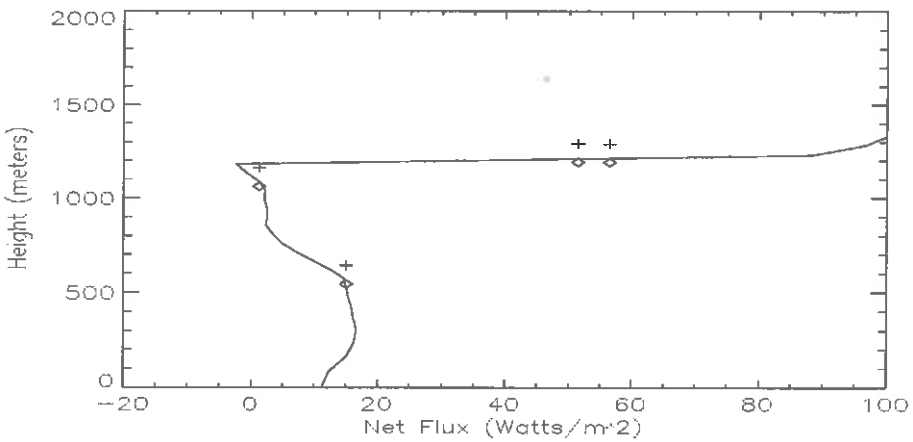

Figure 2: A comparison of observed and predicted net longwave fluxes through a sheet of stratocumulus. The solid line shows the net fluxes predicted by the longwave radiation scheme within the cloud model. The crosses show the net fluxes observed by the C-130 aircraft while the diamond symbols show the observed net fluxes plotted with their height assignments reduced by 100 meters.

Most works have highlighted two mechanisms for the longwave radiative forcing; large scale cooling of the troposphere, and preferential cooling of the clear air around the clouds leading to weak convergence into the cloudy air. Another possible mechanism is radiative destabilization due to cloud top cooling and cloud base warming. This latter mechanism is likely to be very sensitive to the vertical resolution of the grid. Two dimensional simulations of a tropical squall are being performed to determine the impact of longwave radiation. Results from these simulations also show that LW radiation does significantly enhance the total rainfall. Sensitivity studies will be performed to determine the relative importance of the forcing mechanisms and the effect of grid resolution on the radiative effects. Experiments will also be performed to determine the effect of the improvements to the treatment of cloud ice and the inclusion of absorption by rain within the radiative scheme.

We have recently made our first comparison experiments with the single column version of the Met Office unified climate and NWP model (in collaboration with David Gregory of the Hadley Centre), to test the convective parametrization scheme in that model. So far we have only simulated one convective regime, a mid-latitude cold-air outbreak, but preliminary results are interesting and encouraging. They show the importance of getting the balance right between transports by two competing parametrizations in the unified model: the 'rapidly mixing' boundary layer and deep convection schemes. They also show that it may be possible to use the cloud model to tune some of the parameters in the convective parametrization (eg entrainment rates).

We have also used the same sequence of simulations of an idealised cold-air outbreak to investigate momentum transport and gravity wave generation by deep convection. Within this small area of parameter space, both of these processes can be parametrized in terms of the shear and some measure of the convective activity. For gravity wave generation, linear theory gives us a basis for the parametrization and the hope that we can use it in different convective regimes. Momentum transport by convection can be up gradient or down gradient in different regimes so its parametrization in a climate or NWP model is more problematic.

The interaction of convective downdraughts with the surface is another area of study. We have done some preliminary work on the generation of gusts by deep convection, looking at the relative importance of two processes: downward advection of horizontal momentum, and deflection of the downdraught by the surface. Both mechanisms are important in our simulations, and the results can be interpreted using a simple theory based on energy arguments. This work may lead to a scheme for estimating gusts in NWP models. In future work we will investigate the interaction of gusts and surface fluxes.

References

Derbyshire S.H. and Kershaw R., 1993. Turbulence simulation in the Met Office. *Met Mag*, **122**, 25-34.

Dharssi I., 1994. The effect of rain on longwave radiation. *Internal Report*, **No. 9**,

JCMM.

Dudhia J., 1989. Numerical study of convection observed during the Winter Monsoon Experiment using a mesoscale two-dimensional model. *J. Atmos. Sci.*, **36**, 586-601.

Edwards J.M., 1992. Implementing the two-stream equations in the radiation code. Personal communication.

Ingrams W.J., 1993. Radiation. Unified model documentation paper 23. United Kingdom Meteorological Office.

Lin Y-L., Farley R.D. and Orville H.D., 1983. Bulk parametrization of the snow field in a cloud model. *JCAM*, **22**, 1065-1092.

Shutts, G., 1991. Liquid water static energy — a moist thermodynamic variable for use in numerical models. *Mesoscale Modelling Newsletter*, **No. 3**, JCMM, 36-41.

Slingo A. and Wilderspin R.C., 1986. Development of a revised longwave radiation scheme for an atmospheric general circulation model. *Q.J.R. Met. Soc.*, **112**, 371-386.

Stephens G.L., 1984. The parameterization of radiation for numerical weather prediction and climate models. *Mon. Wea. Rev.*, **112**, 826-867.

Sun Z. and Shine K.P., 1993. Studies of radiative properties of ice and mixed phase clouds. *Submitted to Q.J.R. Met. Soc.*

Swann, H.A., 1993. Modelling convective systems on the Large Eddy Simulation Model. *Mesoscale Modelling Newsletter*, **No. 4**, JCMM, 41-49.

Swann, H.A., 1994. Cloud microphysical processes — a description of the parametrization used in the Large Eddy Model. *Internal Report*, **No. 10**, JCMM.

Tao W.K., Simpson J., Sui C.H., Ferrier B., Lang S., Scala J., Chou M.D. and Pickering K., 1993. Heating, moisture and water budgets of tropical and midlatitude squall lines: comparison and sensitivity to longwave radiation. *J. Atmos. Sci.*, **50**, 673-690.

Numerical Modelling Study Of The Balanced Flow Following Localized Deep Convection

Mike Gray

Abstract

The Met Office Large Eddy Model is used to simulate the geostrophic adjustment process following the growth of a deep convective plume. Focus is concentrated upon the partitioning of energy between balanced flow, gravity waves and dissipation, and how this changes with the quantity of mass convected by the plume. In contrast to previous experiments a Coriolis parameter f of $10^{-4}\,s^{-1}$ is used; this is made possible by the use of a stretched horizontal grid in the code. The 2-D simulations demonstrate a clear relationship between the convected mass and the energy trapped in the balanced flow, and that these values can approach **60 %** of the total energy released.

1 Introduction

Deep convection can be considered as a transfer of mass from one part of the atmosphere to another, *e.g.* the boundary layer to the mid-troposphere. One problem, considered by Shutts (1987), is to determine the balanced flow state in the presence of a rotating environment. The solution is an anticyclonic flow around the lens region of convected mass with a vertical shear line front from where the mass had originated. Shutts and Gray (to appear, hereinafter referred to as SG) extended this notion by studying the adjustment following a deep convective plume in a numerical model. These experiments were conducted in 2-D with an artificially high rotation rate ($f = 10^{-3}\,s^{-1}$) but, nonetheless, indicated that :

(a) Over a third of the released energy was trapped in the balanced flow.

(b) The energy partitioning between balanced flow, gravity waves and dissipation for constant convected mass was sensitive to the domain size.

(c) The total energy released and the balanced energy can be considered as simple functions of convected mass.

The proportions of balanced energy trapped were much higher than those from other studies (e.g. Schubert et al, 1980). The successful analytic model of SG gave cause to believe that these results would also be observed for simulations with $f = 10^{-4}\,s^{-1}$. However, this involves scaling everything up such that the convected mass lens would be of a similar number of Rossby deformation radii (R). This quantity is inversely proportional

to f, so that in an $f = 10^{-4}\,s^{-1}$ run everything would have to be ten times larger. The conclusion of (b) causes some problems. In order to have sufficient R in the domain such that the partitioning of energy is no longer affected by the domain boundaries the domain would have to be 2000 km wide. Using the same number of gridpoints as in SG (1000×180) this would require a horizontal grid spacing of 2 km which is too large to effectively simulate the deep convective plume. Increasing the number of grid points is not a possibility due to computational constraint and so for the following experiments a horizontally stretched grid is used.

Result (c) from SG was determined by considering simple scaling arguments. The two expressions were :

$$E_B \propto {M_C}^2 \tag{1}$$

and

$$E_T = C_0 M_C - \left(\frac{2}{3}\right) \eta {M_c}^{3/2} \tag{2}$$

where E_B is the balanced energy, E_T is the total energy released, M_C is the convected mass, C_0 is the initial CAPE and η is an unknown constant which reflects how much CAPE has been eroded by subsidence. A maximum size for M_C is postulated in SG for when $E_B = E_T$. Only a few tentative runs had been conducted with varying M_C; of primary interest is to validate qualitatively expressions (1) and (2). A succession of convective plume experiments are conducted, in which the amount of mass convected is allowed to vary between runs, whilst keeping other parameters constant.

2 Model Formulation

The model used is the same as described in SG, namely a large eddy resolving model, based on the Boussinesq, anelastic equations of motion. Moist processes are represented using a liquid water static energy variable (Shutts, 1991) and instant precipitation (the immediate removal of liquid water upon formation with no evaporative effects). The model is used in 2-D with stretched grids in both the vertical and horizontal.

The horizontal stretched grid precludes the use of fast Fourier transforms in the pressure solver so a different approach must be used. The one adopted is that of Farnell (1980) in which a transformation analogous to the Fourier one is made but which uses eigenvectors appropriate to the stretched grid. The decision is use this method was based on the success that had been achieved with its use in other models, in particular, that of Wood and Mason (1993). For the simulations described the horizontal grid spacing increases smoothly from 200 m in the centre of the domain, where the convective plume is initiated, to 6 km at the peripheries ($X = \pm 1000\,km$). This larger grid spacing is still ample to resolve the gravity waves produced. Vertical grid spacing is 70 m up to 10 km, where an 8 km damping layer starts, in which resolution increases to 160 m.

The model is initialised with a constant static stability, $N^2 = 1.4 \times 10^{-4}\,s^{-2}$ which with a bottom level temperature of 291 K provides a CAPE of just over 500 J. An initial bubble of diameter 2 km, 0.5 K warmer than the environment, is centred in the domain to provide the impetus for the convective plume. The initial moisture fields for the simulations are

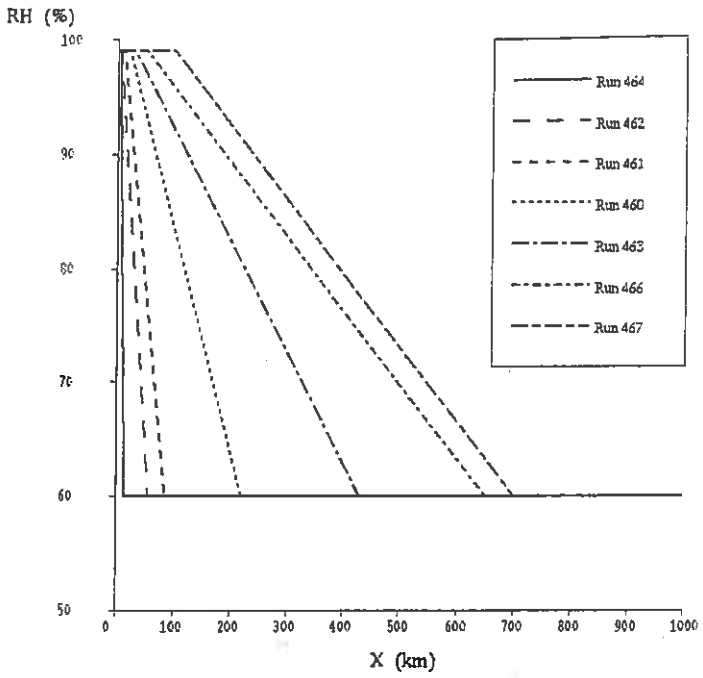

Figure 1: Initial state relative humidity fields at $z = 0\,\mathrm{m}$

shown in Figure 1; a central block of 99 % relative humidity tails off to a background 60 % at the domain boundary. This also decreases vertically to the same background level. Restricting the available moisture in this way allows a degree of control over how much mass is ultimately convected in the plume.

The simulations are run up to a quasi-steady state at 500 000 s. The partitioning of energy into balanced flow, gravity waves and dissipation (*i.e.* that due to the ULTIMATE advection scheme and subgrid processes) is diagnosed in the same way as in SG. The convected mass is estimated by taking the inverse of the resultant potential vorticity field :

$$M_C = -\rho \log\left(\frac{PV_f}{PV_i}\right) \tag{3}$$

where PV_i is the initial potential vorticity, PV_f is the final potential vorticity and ρ is the density. Equation (3) is derived in the usual way for Ertel's potential vorticity, except with a mass forcing function applied to the continuity equation.

3 Results

The values of M_C, E_T and the partitioning of energy into balanced flow, gravity waves and dissipation are shown in Table 1. The proportion of balanced energy increases with M_C, as expected, and there is a compensating decrease in gravity wave energy. The dissipation remains more or less constant at about a quarter, which is less than in SG due to the less dissipative nature of ULTIMATE. The exception is Run 462 in which dissipation is markedly higher. Sensitivity experiments showed that this did not have a numerical

Run	M_C ($\times 10^3$ kg)	E_T (Jm^{-3})	Balanced (%)	Gravity Waves (%)	Dissipation (%)
464	563.2	0.073	7.9	66.7	25.4
462	1632.0	0.217	21.6	43.0	34.9
461	2379.2	0.330	27.9	43.6	28.6
460	5102.4	0.634	43.2	32.3	24.2
463	5627.2	0.695	49.4	26.5	24.1
466	6472.0	0.757	54.7	18.7	26.7
467	6712.0	0.752	58.4	17.6	24.1

Table 1: Convected mass, energy released and partitioning.

cause, but appeared to be related to the scale of the convection.

Examination of the time series of the vertical component of kinetic energy, *i.e.* the intensity of the updraught, show that the convection proceeds in most cases as a succession of short, intense plumes interspersed with a period of slow steady convection. The exceptions are Runs 464 and 462. In Run 464 only one intense plume forms and there is no steady convection; in Run 462 again only one plume forms but this persists as intense steady convection for a much longer time. It is believed that this form of plume may be proportionately more dissipative than the shorter kind.

For the higher M_C runs the proportion of energy going into balanced flow (B) approaches 60 %. B is plotted against M_C in Figure 2, which shows the relationship to be approximately linear. This can be explained by examining equations (1) and (2). If the expression for the balanced energy is divided by that for the total energy it can be shown that :

$$B \propto \frac{M_C^2}{M_C - \gamma {M_C}^{3/2}} \tag{4}$$

where γ is $(2/3)\eta/C_0$. If γ is small then $B \propto M_C$, *i.e.* the erosion of CAPE due to subsidence warming is not particularly significant.

Equations (1) and (2) can be validated on their own. Equation (1) implies that a plot of M_C^2 against E_B should give a straight line whilst equation (2), if γ were assumed to be small, should be linear against M_C. These graphs are shown in Figure 3. In both cases the linear relationship holds, although there is a slight indication that the $-{M_C}^{3/2}$ term may be becoming significant for higher M_C.

4 Discussion

Balanced flow accounted for nearly 60 % of E_T in the higher M_C simulations. This high level suggests that the maximum lens state where $E_T = E_B$ is achievable, although this would have to take into account the 25 % of initial energy released that is dissipated in the plume. Attempts at simulating plumes up to this maximum M_C were unsuccessful, as increasing the region of moisture allowed secondary plumes to develop in the domain, thus polluting the results. It may be that it is not possible to simulate individual lenses of that size. Nevertheless, the lenses simulated were approaching the length scales of observed

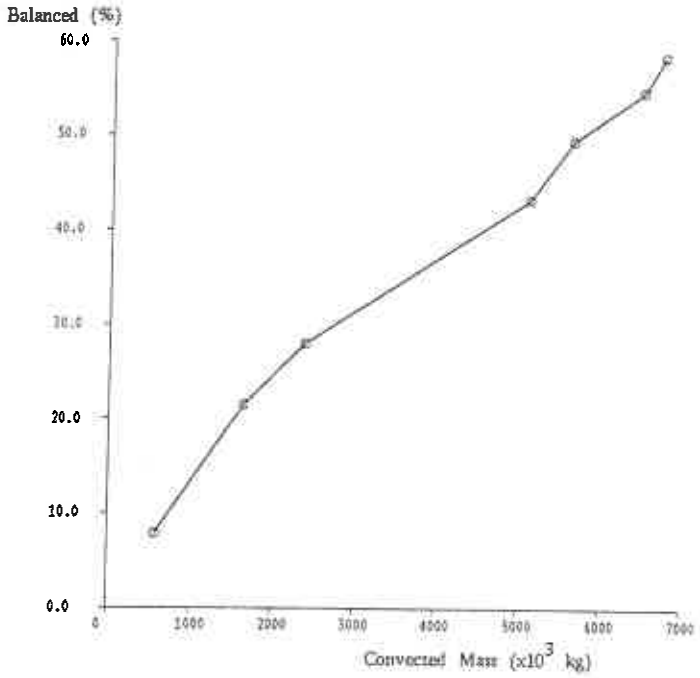

Figure 2: Plot of proportion of balanced energy against convected mass (M_C) for the simulations

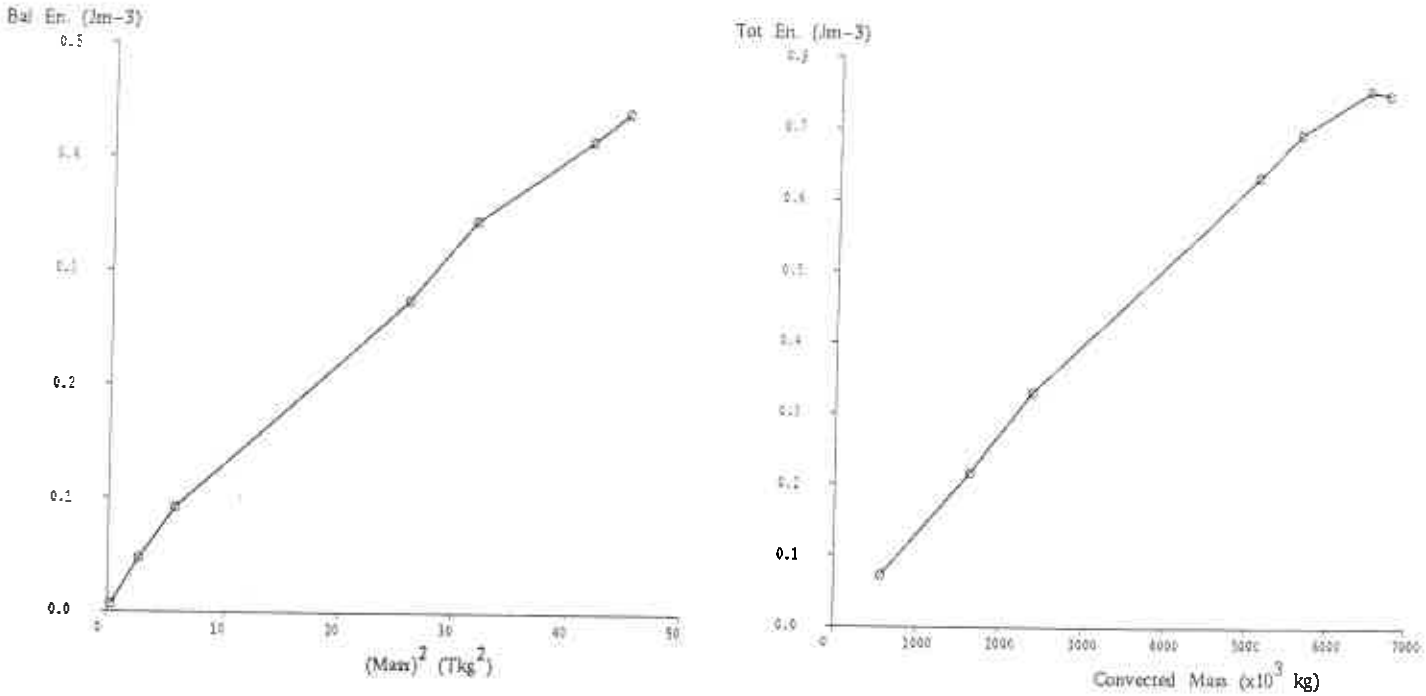

Figure 3: (a) Plot of Balanced Energy against M_C^2. (b) Plot of Total Energy against M_C

Mesoscale Convective Systems, and so the fate of the balanced energy trapped in such systems could have important implications for future parametrizations. The identification of simple relationships between convected mass and balanced energy could be useful in this respect.

However, it must be remembered that these simulations are idealised and only two-dimensional. Questions must be asked about the lens stability to shear, although most MCS profiles show little shear at the lens level, and whether similar results would be repeated in three-dimensions. The development of the stretched horizontal grid will permit such investigation, although artificially high rotation rates may have to be used. But the success of these experiments tend to lend support to the idea that scaling results to different f is valid.

References

Farnell, L. 1980 Solution of Poisson equations on a non-uniform grid. *J. Comput. Phys.*, **35**, 108–425.

Schubert, W.H., J.J. Hack, P.L. Silva Dias and S.R. Fulton 1980 Geostrophic adjustment in an axisymmetric vortex *J. Atmos. Sci.*, **37**, 1464–1484.

Shutts, G. 1987 Balanced flow states resulting from penetrative, slantwise convection. *J. Atmos. Sci.*, **44**, 3363–3376.

Shutts, G. 1991 Liquid Water Static Energy - a moist thermodynamic variable for use in numerical models. *JCMM Mesoscale Newsletter* **No. 3**

Shutts, G. and M.E.B. Gray 1994 A numerical modelling study of the geostrophic adjustment process following deep convection. *Quart. J. Roy. Meteor. Soc.* *To appear*

Wood, N. and P. Mason 1993 The pressure force induced by neutral turbulent flow over hills. *Quart. J. Roy. Meteor. Soc.*, **119**, 1233–1267.

Progress report on the use of the Clark Mesoscale Model as applied to Northern England

Alan Gadian[+], Richard Lord[+] and Jutta Thielen[*]
Physics, UMIST[+] and Dept. of Env. Science, University of Lancaster[*]

Introduction.

The Clark(1977) anelastic mesoscale model, has been continually developed over recent years to include the facilities of high resolution inner nested domains, Ekman surface frictional effects, warm Kessler(1969) microphysics and ice phase representations (Koenig and Murray, 1976). This report will give a very brief description of some preliminary results obtained from **(a)** simulations of airflow and cap cloud formation over Great Dun Fell and **(b)** topographically influenced convection in Northern England. Only a small part of the modelling studies being carried out using this model, are presented here.

A major original aim of this work was to examine and improve the microphysical representation of input water and ice spectra, as these directly influence the growth of precipitation. The total water content of clouds is largely determined by the large scale thermodynamical structure and dynamics, but the number density and maximum cloud size are cloud type and origin dependent. Continental cumulus have high number densities ~ $400cm^{-3}$ and a low rmax ~ $10\mu m$, whereas maritime cumulus have ~ $75cm^{-3}$ and a larger rmax ~ $20\mu m$ for similar water contents of $0.5gm^{-3}$. Stratus clouds have approximately half the number densities and twice the maximum radii of their respective origin cumulus types. The preliminary results shown below, use the original microphysical formulations for warm and ice water phases and although the consequences of different droplet spectra are being investigated.

Cap Clouds over Great Dun Fell

Figures 1 display a very limited sample of the results of model simulations of airflow over Cumbria in Northern England. The Ribble valley provides the Southern boundary, and the Forth river the Northern edge. The outer contours on figures (a) and (b) show the coastline, with topographical contours displayed at 207.5m intervals. Contour intervals, field maxima and minima, and time are shown above and below each diagram. A cap cloud, or more realistically a haze, is visible on these figures, but is observed to develop and then vanish on time periods of 400 seconds. After 2000 seconds a stationary pattern develops.

There were no accurate measurements corresponding to this simulation, but it was apparent from observations, that the cloud was much thicker than these results suggest. The model vertical resolution of 500m was too large to describe the cap cloud (the inner nested model horizontal was set at 4 km) The vertical velocities either side of the summit of Great Dun Fell, positioned to the centre of the frames (figures 1(c) and 1(d)), and to the right of the Lune valley, indicate that marginally reduced cloud concentrations on the lee may partly be due to deposition, but not a significant factor on the upwind slopes. It is apparent that the initial Marshall-Palmer droplet spectra affects the details of the cap cloud, and, is being currently examined in addition to the vertical resolution.

Topographical Influence of the Pennines on Convection

These model simulations were aimed at investigating the effects of the Pennine topography on the development of convection, given differing wind conditions. This research is being submitted for publication, and again only a very brief summary is presented here.

The model was used in a similar form to that above, except that the inner nested region had a horizontal grid step of 2 km. Figure 2 displays the domains of the nested models. In addition, the surface solar flux conversion rate μ was varied to include a thermal land forcing of 30%, urban heat islands forcing of 40%, with rivers and lakes set to 20%. In order to produce a strong sea breeze or convergent flow, in certain simulations the conversion rate was set to zero over the sea (compared with commonly used values, as in the section above, of 10%).

Two particular case studies of convective storms were analysed using a Tϕ diagram from Aughton on the morning of 19th May 1989. In fact the sounding was very similar to that on the 24th May 1989 which produced the Toddbrook storm. In the earlier, so called Halifax storm, the winds were predominantly from the West or South West, but in the second, the winds below 800 mb were from the South, and more westerly above. (see also Swann 1993, for another study of this storm)

The Toddbrook storm started about noon and lasted two hours, as produced in the simulation. The rainfall rates and locations agree well, with the northwards movement being described well in the computations, although the model did produce much convection to the East of the Pennines, which is not visible on the limited data available. Inclusion of the urban heat island forcing made the results less realistic, but as Oke(1978) suggests, their effects should only be included in the afternoons and evenings.

The Halifax storm was much more intense, and lasted 7 hours compared with the models 2 hours. Despite this, the favoured location for the development of the storm was the same in the simulation and observations. The initial stages were well simulated, but the model failed to produce the stationary phase and the convection on the eastern slopes of the Pennines. It is apparent that the storm had other forcing mechanisms for the convection which the model did not have. The resolution of radiosonde data is insufficient to quantify the large scale convergence which may have been present in synoptic weather situation, and which could apply additional forcing.

The results for these two simulations, and many others, all indicate the very significant effect of the topography, the forced lifting and the urban heat island effects have on the mesoscale meteorology of Northern England. Full details of these simulations are being submitted for publication shortly.

References:

Clark, T.L. (1977) *A small-scale dynamic model using a terrain following co-ordinate transformation* J.Comp.Phys, 24, pp 186-215

Kessler, E. (1969) *On the distribution and continuity of water substance in atmospheric circulation's* Met. Monographs, 10, 32, pp1-83

Koenig, L.R. and Murray F.W. (1976) *Ice-bearing cumulus cloud evolution, Numerical simulation and general comparison against observation* J.Appl. Met, 15, pp747-67

Oke, T.R. (1978) *Boundary Layer Climates*, Methuen & Co. London

Swann, H. (1993) *Modelling Convective Systems on the Large Eddy Simulation Model* JCMM newsletter 4, February 1993

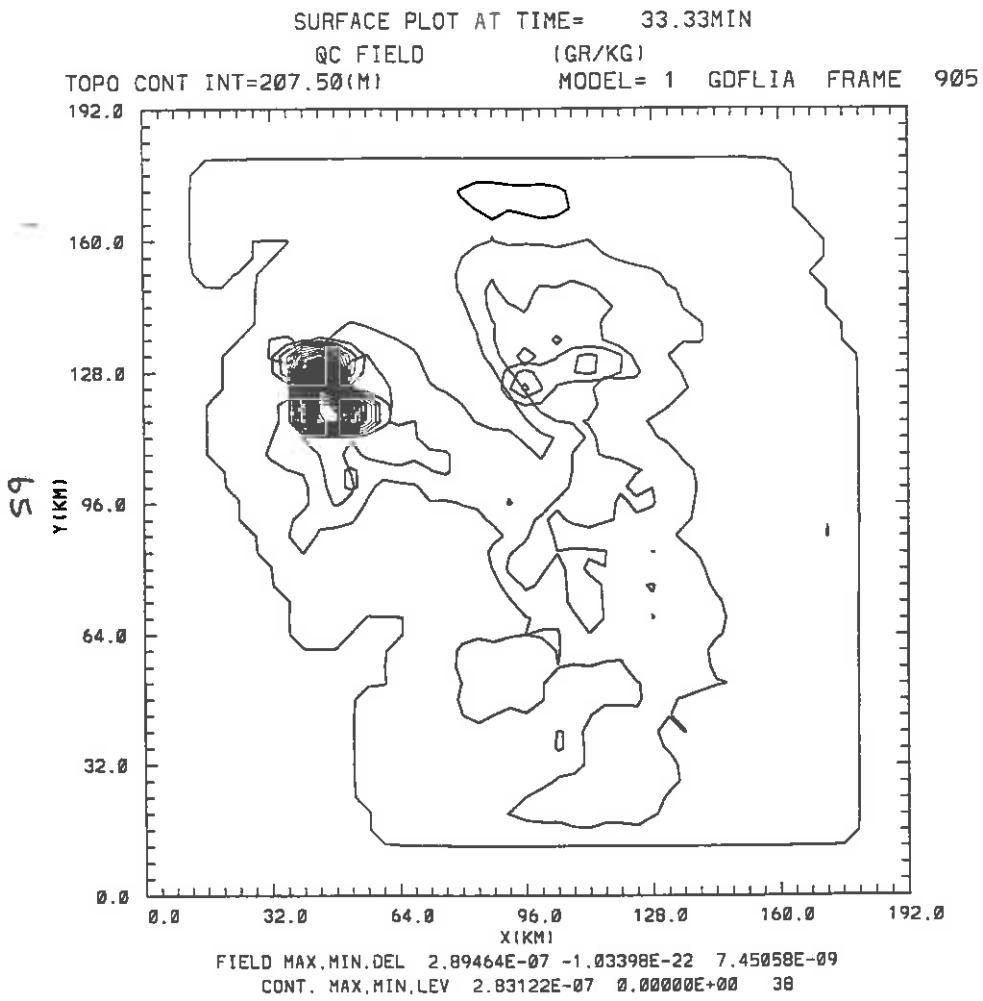

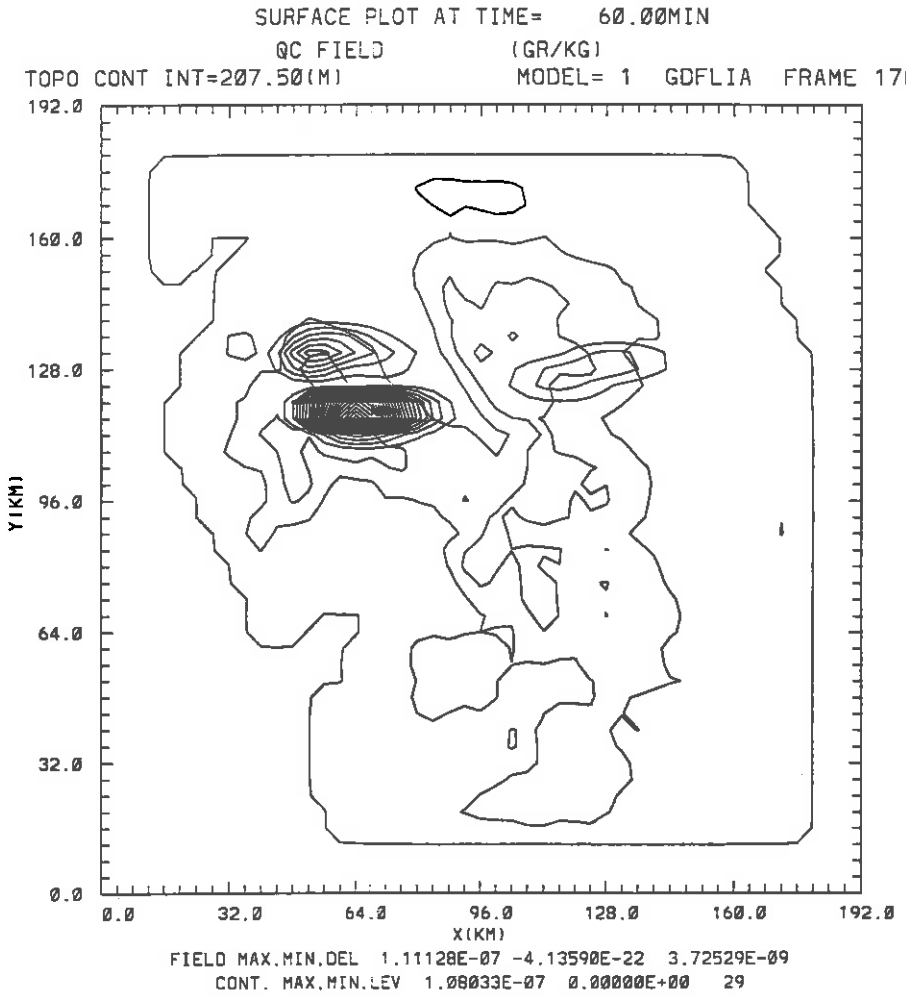

Figures 1 (a) & (b). Contours of cloud mixing ratio imposed on topographical contours, after 33 and 60 model minutes.

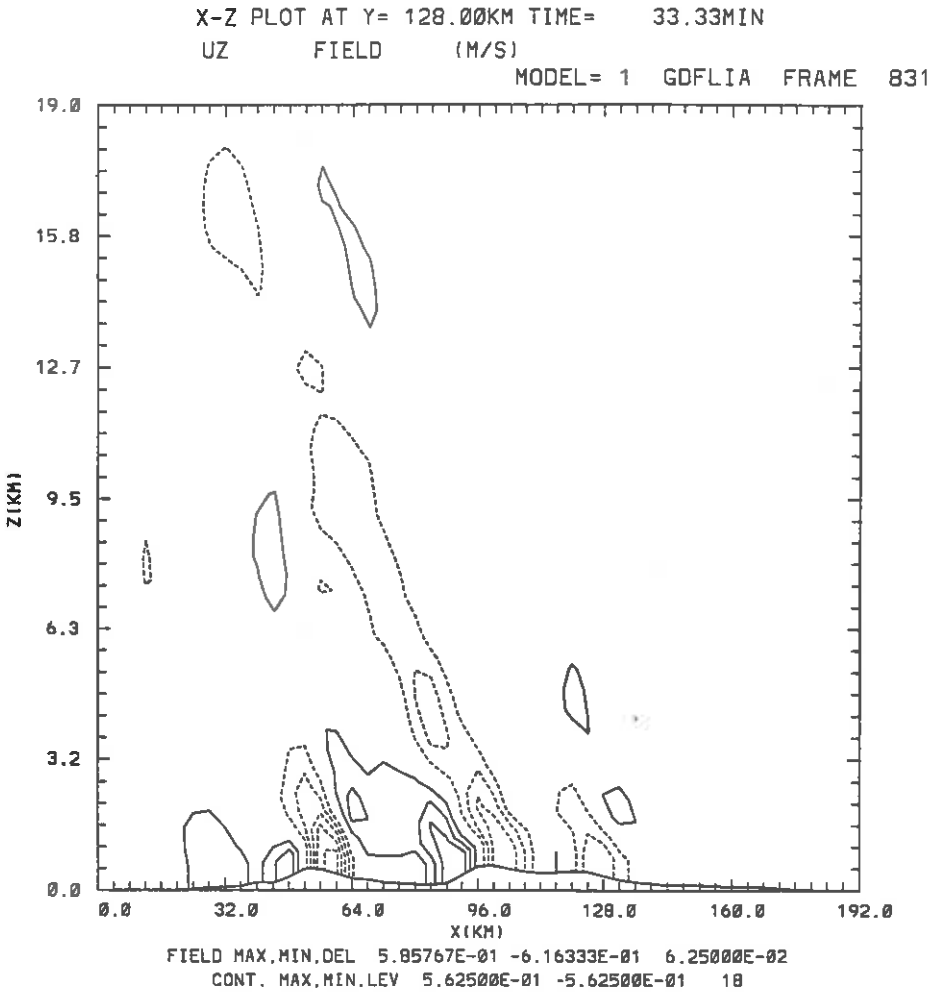

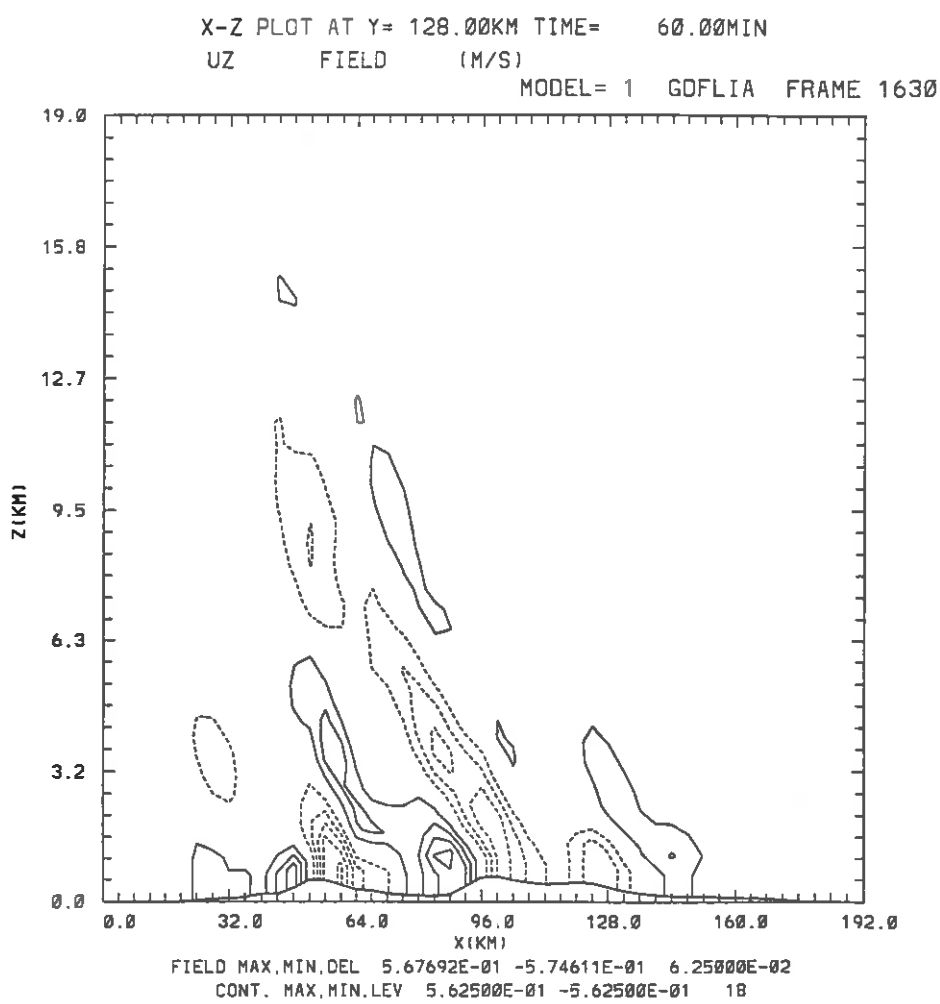

Figures 1(c) & (d). Vertical wind speeds from an x z cross section, showing westerly phase tilt with height

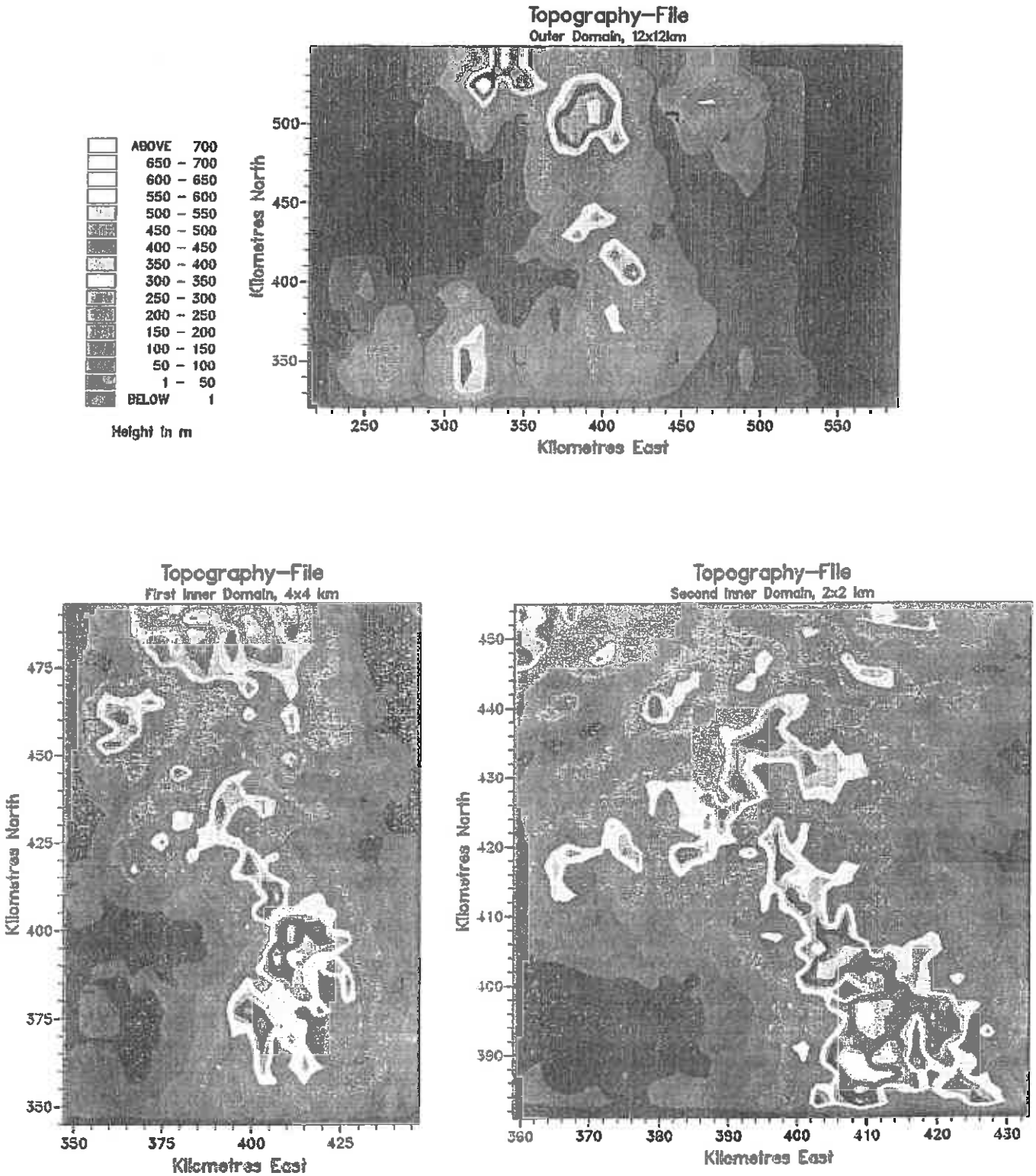

Figure 2: Topography of the three different domains used in the model

CURRENT JCMM INTERNAL REPORTS

This series of JCMM Internal Reports, initiated in 1993, contains unpublished reports and also versions of articles submitted for publication. The complete set of Internal Reports is available from the National Meteorology Library on loan, if required.

1. **Research Strategy and Programme.**
   K A Browning et al
   January 1993

2. **The GEWEX Cloud System Study (GCSS).**
   GEWEX Cloud System Science Team
   January 1993

3. **Evolution of a mesoscale upper tropospheric vorticity maximum and comma cloud from a cloud-free two-dimensional potential vorticity anomaly.**
   K A Browning
   January 1993

4. **The Global Energy and Water Cycle**
   K A Browning
   July 1993

5. **Structure of a midlatitude cyclone before occlusion.**
   K A Browning and N Roberts
   July 1993

6. **Developments in Systems and Tools for Weather Forecasting.**
   K A Browning and G Szejwach
   July 1993

7. **Diagnostic study of a narrow cold frontal rainband and severe winds associated with a stratospheric intrusion.**
   K A Browning and R Reynolds
   August 1993

8. **Survey of perceived priority issues in the parametrizations of cloud-related processes in GCMs.**
   K A Browning
   September 1993

9. **The Effect of Rain on Longwave Radiation.**
   I Dharssi
   September 1993

10. **Cloud Microphysical Processes - A Description of the Parametrization used in the Large Eddy Model.**
    H Swann
    October 1993

11. **An Appreciation of the Meteorological Research of Ernst Kleinschmidt.**
A J Thorpe
May 1992

12. **Potential Vorticity of Flow Along the Alps.**
A J Thorpe, H Volkert and Dietrich Heimann
August 1992

13. **The Representation of Fronts.**
A J Thorpe
January 1993

14. **A Parametrization Scheme for Symmetric Instability: Tests for an Idealised Flow.**
C S Chan and A J Thorpe
February 1993

15. **The Fronts 92 Experiment: a Quicklook Atlas.**
Edited by T D Hewson
November 1993

16. **Frontal wave stability during moist deformation frontogenesis. Part 1. Linear wave dynamics**
C H Bishop and A J Thorpe
May 1993

17. **Frontal wave stability during moist deformation frontogenesis. Part 2. The suppression of non-linear wave development.**
C H Bishop and A J Thorpe
May 1993

18. **Gravity waves in sheared ducts.**
S Monserrat and A J Thorpe
October 1993

19. **Potential Vorticity and the Electrostatics Analogy: Quasi-Geostrophic Theory.**
C Bishop and A J Thorpe
November 1993

20. **Recent Advances in the Measurement of Precipitation by Radar.**
A J Illingworth
April 1993

21. **Micro-Physique et Givrage. Cloud Microphysics and Aircraft Icing.**
A J Illingworth
May 1993

22. **Differential Phase Measurements of Precipitation.**
M Blackman and A J Illingworth
May 1993

23. **Estimation of Effective Radius of Cloud Particles from the Radar Reflectivity.**
N I Fox and A J Illingworth
May 1993

24. **A Simple Method of Dopplerising a Pulsed Magnetron Radar.**
L Hua, A J Illingworth and J Eastment
November 1993

25. **Radiation and Polar Lows.**
George C Craig
February 1994

26. **Collected preprints submitted to International Symposium on the Life Cycles of Extratropical Cyclones; Bergen, Norway, 27 June - 1 July 1994**
April 1994

27. **Convective Frontogenesis**
Douglas J Parker and Alan J Thorpe
April 1994

28. **Improved Measurement Of The Ice Water Content In Cirrus Using A Total Water Evaporator**
Philip R A Brown and Peter N Francis
April 1994

29. **Mesoscale Effects of a Dry Intrusion within a Vigorous Cyclone**
K A Browning and B W Golding
April 1994

30. **GEWEX Cloud System Study, Science Plan**
May 1994

31. **Parametrization of Momentum Transport by Convectively Generated Gravity Waves**
R Kershaw
May 1994

32. **Mesoscale Modelling Newsletter, No. 5**
May 1994

Met Office Joint Centre for Mesoscale Meteorology Department of Meteorology
University of Reading PO Box 243 Reading RG6 6BB United Kingdom
Tel: +44 (0)118 931 8425 Fax: +44 (0)118 931 8791
www.metoffice.com